RMetS

Royal Meteorological Society

Review Article
Droplet growth in warm turbulent clouds

B. J. Devenish,[a][*][†] P. Bartello,[b] J.-L. Brenguier,[c] L. R. Collins,[d] W. W. Grabowski,[e] R. H. A. IJzermans,[f] S. P. Malinowski,[g] M. W. Reeks,[f] J. C. Vassilicos,[h] L.-P. Wang[i] and Z. Warhaft[d,j]

[a]*Met Office, Exeter, UK*
[b]*McGill University, Montreal, Quebec, Canada*
[c]*Météo-France/CNRS, GAME/CNRM, Toulouse, France*
[d]*Sibley School of Mechanical and Aerospace Engineering, Cornell University, Ithaca, New York, USA*
[e]*National Center for Atmospheric Research, Boulder, Colorado, USA*
[f]*School of Mechanical and Systems Engineering, University of Newcastle, Newcastle-upon-Tyne, UK*
[g]*University of Warsaw, Faculty of Physics, Institute of Geophysics, Warsaw, Poland*
[h]*Institute for Mathematical Science and Department of Aeronautics, Imperial College London, UK*
[i]*Department of Mechanical Engineering, University of Delaware, Newark, Delaware, USA*
[j]*Atkinson Center For a Sustainable Future, Cornell University, Ithaca, New York, USA*

[*]Correspondence to: B. J. Devenish, Met Office, Fitzroy Road, Exeter EX1 3PB, UK.
E-mail: ben.devenish@metoffice.gov.uk
[†]The contribution of these authors was written in the course of their employment at the Met Office, UK, and is published with the permission of the Controller of HMSO and the Queen's Printer for Scotland.

In this survey we consider the impact of turbulence on cloud formation from the cloud scale to the droplet scale. We assess progress in understanding the effect of turbulence on the condensational and collisional growth of droplets and the effect of entrainment and mixing on the droplet spectrum. The increasing power of computers and better experimental and observational techniques allow for a much more detailed study of these processes than was hitherto possible. However, much of the research necessarily remains idealized and we argue that it is those studies which include such fundamental characteristics of clouds as droplet sedimentation and latent heating that are most relevant to clouds. Nevertheless, the large body of research over the last decade is beginning to allow tentative conclusions to be made. For example, it is unlikely that small-scale turbulent eddies (i.e. not the energy-containing eddies) alone are responsible for broadening the droplet size spectrum during the initial stage of droplet growth due to condensation. It is likely, though, that small-scale turbulence plays a significant role in the growth of droplets through collisions and coalescence. Moreover, it has been possible through detailed numerical simulations to assess the relative importance of different processes to the turbulent collision kernel and how this varies in the parameter space that is important to clouds. The focus of research on the role of turbulence in condensational and collisional growth has tended to ignore the effect of entrainment and mixing and it is arguable that they play at least as important a role in the evolution of the droplet spectrum. We consider the role of turbulence in the mixing of dry and cloudy air, methods of quantifying this mixing and the effect that it has on the droplet spectrum. Copyright © 2012 Royal Meteorological Society and British Crown Copyright, the Met Office

1. Introduction

Rainfall from 'warm clouds' (with cloud top below the freezing level) accounts for approximately 30% of the total rainfall on the planet and approximately 70% of all rainfall in the Tropics (Lau and Wu, 2003). The interaction of cloud and raindrops with radiation plays a significant role in driving the atmospheric circulation, and hence the correct representation of cloud microphysics in general circulation models for numerical weather and climate prediction is of obvious importance. Of course, the complexity of the physical processes involved and the vast range of scales mean that what form the 'correct' representation should take is subject to considerable uncertainty, not least because of the role of turbulence in the formation of clouds and precipitation.

Turbulence is integral to the formation of clouds and precipitation, yet its role, particularly at the smallest scales, is often not well appreciated in the cloud physics community. The difficulty in measuring clouds at small scales, and the lack of realistic cloud models that span all the relevant scales, mean that its precise effect is hard to quantify and makes an assessment of its importance difficult. However, increasing computer power, more sophisticated laboratory experiments and better observations have all brought a resurgence of interest in this issue in recent years, particularly from the turbulence community. The phenomenon of preferential concentration, also referred to as segregation or clustering, of droplets has perhaps received most attention from the turbulence community, yet this is just one of many processes at work in clouds: large-scale atmospheric stability, aerosols and entrainment all play important roles in the formation of clouds.

As a result of their inertia, droplets do not follow the flow exactly and tend to be non-uniformly distributed in a turbulent flow. Direct numerical simulations (DNS) of incompressible turbulence have provided a clear demonstration of the clustering of inertial particles when the particles respond to changes in the turbulent flow on the same time-scale as the smallest eddies change (e.g. Squires and Eaton, 1990; Wang and Maxey, 1993; Sundaram and Collins, 1997). Thus collision rates in a turbulent flow may be enhanced relative to a quiescent one. However, the extrapolation of these results to real clouds is not guaranteed: as pointed out by, for example, Grabowski and Vaillancourt (1999), Vaillancourt and Yau (2000), Wang *et al.* (2006a) and Khain *et al.* (2007), many DNS studies have been conducted without gravity, at moderate Reynolds numbers, for much higher energy dissipation rates than is typical of clouds, for equally sized droplets (a *monodisperse* suspension) and for relatively high droplet concentrations compared with typical concentrations in clouds. Perhaps this is not surprising given the difficulty in determining what the relevant parameters are and their values in real clouds. While they are better known today compared with even a decade ago, they remain a subject of continuing research. Clearly, idealized studies of clouds are of most relevance when they are tailored to model real clouds as closely as possible while allowing for the not inconsiderable uncertainty. It is important, then, to understand the assumptions made in DNS and parametrizations of turbulent collision kernels as otherwise collision rates can be overestimated.

Despite the criticisms levelled at idealized studies of clouds and DNS in particular, they remain a valuable tool for understanding the different physical processes involved in their formation in so far as they can be distinguished. However, this means that a meaningful comparison with observations is often difficult because idealized studies, by their nature, focus on a few, or even one, part of the cloud formation process. Nevertheless, it is likely that only through successively more complex but still relatively idealized studies will it be possible to distinguish those physical processes which play a key role in cloud formation and precipitation, and which need to be included in parametrizations of cloud microphysics, from processes which can be regarded as being of secondary importance. An example is DNS of sedimenting cloud droplets (Franklin *et al.*, 2007; Ayala *et al.*, 2008a; Wang *et al.*, 2008) which provided quantitative data on turbulent enhancement of the collision kernel and, more importantly, on the relative contributions to this enhancement from the effects of turbulence on the relative velocity of the droplets, preferential concentration and collision efficiency.

Both theoretical and practical approaches to modelling and understanding turbulent flows typically invoke a wide separation of scales (into various asymptotic regimes, e.g. the viscous dissipation range and the inertial subrange, encompassing a continuum of scales). We follow the conventional statistical description of stationary homogeneous isotropic turbulence (e.g. Monin and Yaglom, 1975): by large-scale turbulence we mean the energy-containing eddies that are influenced by the forcing of the flow and the boundary conditions; by small-scale turbulence we mean those eddies that are often assumed to have universal properties independent of the forcing and the boundary conditions–the smallest of these small-scale eddies have sizes where viscous dissipation acts directly. Although we still do not have detailed evidence for the universal structure of turbulence in warm cumulus clouds, the statistics of turbulence observed in stratocumulus show similar scalings to those observed in laboratory wind tunnel experiments (Siebert *et al.*, 2010a); the higher Reynolds number of cumulus clouds suggests that these scalings are likely to occur there too. This opens the possibility that the theoretical, computational and experimental studies to be described below will have some relevance to cloud physics. However, the effects of large-scale time-dependent inhomogeneities and multi-scale energy exchange between the moist air and liquid droplets could potentially complicate any universal behaviour that is associated with single-phase high-Reynolds number turbulence.

In the next section of this review we consider turbulence at the cloud scale, in particular the sources of cloud turbulence and the effect of entrainment and mixing of dry air (here taken to be cloud-free air with a non-zero water vapour content) on the structure of the cloud. In section 3 we consider theories of droplet growth when the effects of small-scale turbulence and entrainment are neglected and how well observations support these ideas. The effects of small-scale turbulence on the growth of droplets in the absence of entrainment are considered in section 4 and the effect of entrainment on the droplet spectrum is the subject of section 5.

2. Cloud-scale turbulence

The intensity of turbulence in clouds varies widely depending on the cloud type and the stage in its evolution. Most estimates of the parameters that characterize warm turbulent clouds come from a limited number of measurements at low resolution (e.g. MacPherson and Isaac, 1977; Caughey *et al.*, 1982; Pruppacher and Klett, 1997, sections 2.1.3 and 14.5.2) giving typical values of the mean turbulent kinetic energy dissipation rate, ε, of order 10 cm^2 s^{-3} for stratocumulus and 100 cm^2 s^{-3} for small cumulus clouds. Only recently have higher-resolution ($\sim$20 cm) measurements been possible: Siebert *et al.* (2010a) measured $\varepsilon \sim 1$ cm^2 s^{-3} in stratocumulus and Siebert *et al.* (2006a) measured $\varepsilon \sim 10$ cm^2 s^{-3} in small cumulus clouds. The Taylor-scale Reynolds number, R_λ, varies correspondingly between stratocumulus and cumulus: $R_\lambda \sim 5000$ in stratocumulus (Siebert *et al.*, 2010a) and $R_\lambda \sim 30\,000$–$40\,000$ in cumulus (Siebert *et al.*, 2006a). These values of ε can be misleading in that they give no indication of the extremely large fluctuations in the local dissipation rate that are possible: for example, in small cumulus clouds Siebert *et al.* (2006b) found that the dissipation rate could vary by a factor of 50 over scales of order 15 m (see Figure 5 therein); Meischner *et al.* (2001) also found that the dissipation rate could vary by several orders of magnitude on scales of order 100 m within thunderstorm anvils.

2.1. Sources of cloud turbulence

From the perspective of fluid mechanics, the fact that shallow convective clouds, such as boundary-layer cumulus or stratocumulus, are turbulent should not be surprising. This is because the Reynolds number characterizing such flows is much higher than what is traditionally considered a critical Reynolds number for transition to turbulence (between a few thousand and several tens of thousands depending on the details of the flow and the way in which the velocity and length scales are selected). If one assumes that the velocity and length scales representative of shallow convective clouds are of order 1 m s^{-1} and 100 m respectively (both conservative estimates), then the Reynolds number based on the molecular viscosity of air is of order 10^7, which ensures a turbulent flow (unless suppressed by, for example, stable stratification).

The initial seed for the flow instabilities of a small cumulus cloud updraught is likely to originate from the turbulent boundary layer. Both aircraft observations and model simulations (e.g. Miao *et al.*, 2006) clearly show that what is visible as a small convective cloud has a clearly defined updraught emanating from the boundary layer. However, the air just below the cloud base is typically characterized by turbulence levels much smaller than those inside the cloud (MacPherson and Isaac, 1977). Furthermore, ε shows systematic variation with height: measurements of cumulus clouds by MacPherson and Isaac (1977) and Gerber *et al.* (2008) show that ε tends to peak near the cloud top. In addition, one might anticipate that the turbulence intensity should be highest near the cloud edge where turbulent entrainment and mixing between the cloudy air and subsaturated (and typically non-turbulent) air take place (e.g. Siebert *et al.*, 2006a, 2006b). Numerical simulations by Seifert *et al.* (2010) show that ε reaches a maximum near the cloud top at its windward edge (see Figure 6 therein).

Numerical simulations highlight the role of the so-called cloud–environment interface instabilities in cumulus entrainment (Klaassen and Clark, 1985; Grabowski and Clark, 1991, 1993a, 1993b; see also a summary in Grabowski, 2000). The key argument is that such instabilities are a fundamental feature of buoyancy-driven high-Reynolds-number flows and are responsible for the characteristic cauliflower-like shape of the rising buoyant fluid. As summarized in Grabowski (2000), the essential aspect of the instability is the shear layer that develops near the interface as the buoyant fluid pushes upward. Because of the deformational flow near the interface, the shear layer collapses and becomes unstable. Both shear and buoyancy production are important for the kinetic energy of the instability, with buoyancy dominating near the top and shear dominating near the sides (i.e. away from the top). In reality, the interfacial instabilities are a combination of Rayleigh–Taylor and Kelvin–Helmholtz instabilities occurring in a complex geometric set-up. Evolution of the instabilities results in the development of the turbulent transition layer that separates undiluted fluid from the environment. The turbulence that develops (see section 5 in Grabowski and Clark, 1993a, for a detailed discussion) bears strong similarities to homogeneous isotropic turbulence.

2.2. Entrainment and mixing processes

When a turbulent fluid penetrates another fluid with a different density, the turbulent fluid entrains and then mixes this fluid. This is perhaps most clearly seen for a buoyant fluid emanating from an isolated source such as a fire-generated plume. Clouds are also examples of turbulent fluids whose density differs from that of the surrounding fluid and, as such, entrainment is a key process in the dynamics of clouds. Simple models of entrainment at the cloud scale have been relatively successful in parametrizing clouds (e.g. Stevens, 2006) but the rate of entrainment is subject to considerable uncertainty, not least in its dependence on environmental conditions. The nature of entrainment also depends on the cloud type: two cases serve as paradigmatic scenarios in which to study the effect of entrainment on cloud formation and the droplet spectrum, namely isolated cumulus and unbroken stratocumulus. In isolated cumulus, entrainment of dry air occurs throughout the depth of the cloud and results in strong dilution of the cloud: the liquid water content rapidly drops to about 20% of its adiabatic value (Warner, 1955). In unbroken stratocumulus, entrainment proceeds from the top and affects mostly a thin layer (Gerber *et al.*, 2005). By regarding these two cases in a more idealized context, parallels (and differences) may be drawn with entrainment in other buoyancy-driven flows such as dry plumes or thermals which, although not necessarily of direct relevance to real clouds, provides a context for considering more realistic scenarios. It is worth remembering that real clouds form in the context of a turbulent atmosphere with ambient shear and non-uniform stratification and so many permutations of cumulus and stratocumulus are possible. Nevertheless, we briefly consider entrainment in cumulus and stratocumulus separately, more detailed reviews of each case can be found in Blyth (1993) and Stevens (2002) respectively.

2.2.1. Entrainment in cumulus clouds

A simple model for entrainment in a dry plume from an isolated source was proposed by Morton *et al.* (1956), which assumed that the profiles of the buoyancy and vertical velocity are self-similar with height and that the rate of entrainment is proportional to the vertical velocity (and occurs through the lateral edge of the plume). This approach was adapted to modelling entrainment in cumulus clouds (e.g. Morton, 1957; Squires and Turner, 1962) but was less successful for clouds than for dry plumes. Clearly, the latent heating and evaporative cooling that occur within clouds either provide or remove energy that affect the cloud dynamics. Indeed, Morton (1957) showed that when saturation occurs well below the plume top, the dynamics of the cloud are dominated by latent heating rather than the source parameters which characterize dry plumes. Further criticisms of these simple plume models include their inability to predict simultaneously both the vertical extent and liquid water content of the cloud (Warner, 1970) and the assumption of self-similarity, which is only well justified in a neutrally stable environment sufficiently far above the source (see, for example, the discussion in Blyth, 1993).

As the weaknesses of 1-D similarity models of cumulus convection became better understood, an alternative hypothesis grew in importance. Squires (1958) suggested that vertical rather than horizontal entrainment, through penetrative downdraughts into the ascending cloud top, was the primary mechanism for diluting cumulus clouds. While observations by, for example, Paluch (1979) and Jonas (1990) supported this idea, it remains a subject of debate. For example, aircraft observations by Blyth *et al.* (1988) suggest that the entrained air comes primarily from close to, or just above, any of the levels where observations were made. They argued that entrainment from the cloud top cannot account for the observed dilution of cumulus clouds considering the small downward mass fluxes that are observed and the relatively small distances that mixed air parcels are observed to descend. Recently, Heus *et al.* (2008) performed Lagrangian fluid-particle tracking in large-eddy simulations (LES) of cumulus clouds to show that entrainment is primarily lateral rather than through the cloud top. Heus and Jonker (2008) developed this conceptual view of cumulus convection into a model of concentric annuli centred on the cloud core. The cloud core, with positive vertical velocity and buoyancy, is surrounded by a descending shell with negative buoyancy and finally an outer shell representing the ambient dry air. The descending shell forms as a result of evaporative cooling (Turner, 1966) and has been observed in reality (Jonas, 1990; Rodts *et al.*, 2003; Wang *et al.*, 2009) as well as in LES (Heus and Jonker, 2008). Heus and Jonker (2008) argue that lateral entrainment can be reconciled with observations showing that entrained air appears to originate at higher levels by noting that any laterally entrained dry air must be entrained via the descending shell. Implicit in this argument is that the mixing of dry and cloudy air is not instantaneous–a point we return to in section 5.

2.2.2. Entrainment in stratocumulus

Stratocumulus typically forms at a temperature inversion (density interface) capping a mixed layer. An analogous dry situation that provides some insight into entrainment in stratocumulus occurs when a buoyant plume impinges on a density interface. Here the entrainment rate depends on a local Richardson number defined as $Ri = \Delta g' l / w^2$, where $\Delta g'$ is the buoyancy difference across an interface of depth l and w is the velocity of the impacting plume (e.g. Turner, 1973, p. 294). Since entrainment decreases as the stability of the interface increases, the entrainment rate is a decreasing function of Ri. For $Ri \gg 1$, the entrainment rate has been found to vary like $Ri^{-3/2}$, whereas for moderate Ri the entrainment rate decreases like Ri^{-1} (e.g. Turner, 1973, p. 294; Lin and Linden, 2005) and tends to a constant as $Ri \to 0$ (e.g. Lin and Linden, 2005). When the distortion of the interface is taken into account, Mahrt (1979) suggests that the entrainment rate associated with the horizontal and vertical components of the entrainment velocity may differ. However, it is problematic to measure this in practice and illustrates the difficulty in defining the interface and the direction of entrainment–a point we return to in section 5.2. In recent laboratory experiments, however, Gerashchenko *et al.* (2011) have shown the importance of the orientation of the entraining interface with respect to gravity (for a neutrally buoyant flow in the absence of shear) in selectively mixing droplets of different sizes across the interface. These, and the experiments of Good *et al.* (2012), show the importance of the large scales in the entrainment process (although all scales play a role).

The dynamics of dry plumes are dominated by the source parameters; when a plume impinges on the density interface, the dynamics of the small-scale eddies are driven by the dissipation of the larger eddies. In contrast, the dynamics of stratocumulus are, at least in part, controlled by the energy associated with phase changes and radiative cooling because these diabatic processes can force the small-scale eddies directly. Not surprisingly, then, stratocumulus exhibits more complex behaviour than is possible in a dry atmospheric boundary layer. Mixing between cooler saturated air below a temperature inversion and warmer (in the potential temperature sense) subsaturated air above the inversion reduces the temperature difference between the two layers. If the temperature of the resulting mixture is not sufficient to offset any evaporative cooling which accompanies this mixing, then the mixed fluid may have a density which is greater than that of either the lower saturated air or the upper subsaturated air. This is known as *buoyancy reversal* and leads to penetrative downdraughts of dry air occurring at the cloud top (see, for example, Yamaguchi and Randall, 2008). The buoyancy of the mixed fluid is a nonlinear function of the fraction of lower and upper fluid in the mixture and has a minimum at the point where exact saturation occurs (see, for example, Figure 1 of Siems *et al.*, 1990). This observation has led to the concept of *cloud-top entrainment instability* (Deardorff, 1980; Randall, 1980) which, when a critical threshold is passed, may generate a runaway positive feedback between mixing, evaporative cooling and entrainment and in turn lead to the break-up of stratocumulus into cumulus cloud. However, the concept of cloud-top entrainment instability is not necessarily supported by cloud observations because solid stratocumulus is often observed even if the critical threshold is passed (e.g. Figure 1 in Kuo and Schubert, 1988).

Based on studies of aircraft measurements, several authors (e.g. Caughey *et al.*, 1982; Gerber *et al.*, 2005) have suggested the existence of an *entrainment interfacial layer* consisting of previously mixed air in proportions which do not result in

negative buoyancy of the mixed product. This substantially modifies entrainment at the top of stratocumulus. Direct mixing between air from above the inversion and the quasi-adiabatic cloud is not common and the cloud-top entrainment instability criterion should not be applied to free tropospheric air and quasi-adiabatic cloud volumes. More detailed analysis of the small-scale structure of mixing by Haman *et al.* (2007) confirms the presence of an entrainment interfacial layer and mixing between this layer and the cloud. A survey of LES of stratocumulus by Stevens (2002) showed that entrainment rates diagnosed from LES results can vary by up to a factor of two. This has led Stevens *et al.* (2005) to suggest that the entrainment rate may not only be sensitive to the energy-containing eddies but also to the small-scale (subgrid) eddies which are not explicitly resolved in LES, either directly or indirectly through the impact of the small-scale (subgrid) eddies on the large-scale eddies. Such a situation would be in agreement with the concept of an entrainment interfacial layer: since this layer is thin, its dynamics are likely to be dominated by the smaller eddies.

3. Theories and observations of droplet growth

Cloud droplets typically have a radius, a, less than approximately 20 µm, and their number concentrations per unit volume, n, vary from 50 cm^{-3} in maritime clouds to 1000 cm^{-3} in continental clouds (Pruppacher and Klett, 1997, section 2.1.3). For larger droplets, the number concentrations can be less than 1 cm^{-3} (Pruppacher and Klett, 1997, section 2.1.3). The gravitational settling velocities of cloud droplets (with radii less than 20 µm) are typically 4 cm s^{-1} or less (Pruppacher and Klett, 1997, section 10.3.6). Since the typical liquid water content of a small cumulus or stratocumulus cloud is in the range 0.1–1 g m^{-2} (generally higher for cumulus than stratocumulus), it follows that the mass or volume loading is relatively low, the latter being of order 10^{-6} (e.g. Shaw, 2003), and hence that the droplet number concentration is sufficiently dilute that interactions between droplets are infrequent. The low mass loading means that modulation of the turbulence by the droplets is not expected to be significant (e.g. Figure 1 of Elghobashi, 1994). However, droplets do affect the flow field through latent heating and evaporative cooling (see section 4.1) and there is momentum exchange at the droplet scale associated with interactions between droplets which occurs regardless of the larger-scale mass loading.

3.1. Activation and growth of cloud droplets

The formation and growth of cloud droplets may be regarded as a three-stage process: first, droplets are generated by the activation of sub-micron-sized aerosols which act as cloud condensation nuclei (CCN) and typically have a radius of order 0.1 µm (Pruppacher and Klett, 1997, section 9.1). Second, if the conditions allow, the droplets grow to a diameter of a few tens of microns due to condensation. Finally, once the droplets are large enough, they may grow by collision and coalesce with other droplets. The whole process may be described by a continuous function known as the droplet size distribution or spectral density function, $f(a, \mathbf{x}, t)$ where $f \, \mathrm{d}a = \mathrm{d}n$ at position $\mathbf{x}$ and time t, whose evolution is governed by a Boltzmann-type equation (e.g.

Shaw, 2003):

$$\frac{\partial f(a)}{\partial t} + \frac{1}{\rho_a} \nabla \cdot [\rho_a(\mathbf{u} + \mathbf{v}_p(a)) f(a)] + \frac{\partial}{\partial a}(\dot{a} f(a)) =$$
$$J(a) + \frac{1}{2} \int_0^a \frac{a^2}{a''^2} \Gamma_{12}[a'', a'] f(a'') f(a') \, \mathrm{d}a'$$
$$- \int_0^\infty \Gamma_{12}(a, a') f(a) f(a') \, \mathrm{d}a', \quad (1)$$

where $a'' = (a^3 - a'^3)^{1/3}$, $\mathbf{u}$ is the air velocity, $\mathbf{v}_p$ is the droplet velocity, ρ_a is the air density, $\dot{a}$ is the droplet growth rate and Γ_{12} is the collision kernel (see section 4.2). (Note that the dependence of f, $\mathbf{u}$ and $\mathbf{v}_p$ on $\mathbf{x}$ and t has been suppressed for clarity.) The third term on the left-hand side of (1) represents the diffusional growth of droplets due to condensation (which can be thought of as an advection term in radius space). The first term on the right-hand side of (1) represents a source of droplets, the activation rate, J. The second term represents the production of droplets of radius a through coalescence between any two droplets whose masses sum exactly to the mass corresponding to an a-droplet. The last term represents the destruction of droplets of radius a which occurs whenever a droplet of that size coalesces with a droplet of any other size. In the absence of the third term on the left-hand side of (1) and the first term on the right-hand side of the equation, (1) is known as the *stochastic collection equation* or *stochastic coalescence equation* (Smoluchowski, 1916; Pruppacher and Klett, 1997, section 15.3). Note that in meteorological textbooks it is more commonplace to express the part of (1) representing collisions and coalescence in terms of the droplet mass. In the chemical engineering community, equations of the form of (1) are often referred to as population balance equations.

Droplets tend to originate at cloud base where an updraught typically produces a peak in the supersaturation (for moderate updraught velocities). The peak value determines the fraction of available CCN that are activated (Rogers and Yau, 1989, pp. 88, 110). The droplet concentration thus depends on the CCN activation spectrum: clouds growing in a continental or polluted environment typically show higher droplet concentrations than those growing in a marine or pristine environment (Pruppacher and Klett, 1997, section 2.1.3). In a given environment, however, turbulence–more specifically fluctuations in the vertical velocity at cloud base–results in considerable variability of n in a field of convective clouds (Snider *et al.*, 2003). At any location in a convective cloud, the liquid water content ($\propto n\overline{a}^3$, where $\overline{a}$ is the mean droplet radius) is mostly determined by heat and moisture budgets, i.e. it does not depend significantly on the cloud microphysics. The mean droplet radius is therefore smaller in continental or strongly convective clouds than in similar marine or pristine ones, and it scales like $n^{-1/3}$ (Rogers and Yau, 1989, p. 92). Both large droplet radii and large droplet concentrations increase the collision rate, all else being equal. The ubiquitous observation that marine clouds (low droplet concentration) precipitate more readily than continental clouds (high droplet concentration) for equal liquid water contents indicates that the increase in droplet size is more important than the increase in n. Consequently, a local increase in n due to small-scale turbulence could only accelerate the formation of rain if the scaling of the droplet radius like $n^{-1/3}$ is not locally valid, i.e. there is also a small-scale increase in liquid water content.

In some types of clouds, activation of cloud droplets also occurs above the cloud base due to either strongly increasing updraught strength (e.g. Warner, 1969b; Pinsky and Khain, 2002) or entrainment (Warner, 1969a; Paluch and Knight, 1984; Brenguier and Grabowski, 1993; Su *et al.*, 1998; Lasher-Trapp *et al.*, 2005). As discussed in Brenguier and Grabowski (1993, section 3b and Figures 6–8 in particular), entrainment-related activation above the cloud base occurs in vortical structures associated with cloud–environment interface instabilities that bring environmental cloud-free air into the cloud. Modelling studies discussed in Slawinska *et al.* (2011) and Wyszogrodzki *et al.* (2011) show that in-cloud activation leads to approximately constant-in-height mean cloud droplet concentration in shallow cumuli, in agreement with aircraft observations (e.g. Gerber *et al.*, 2008; Arabas *et al.*, 2009) but in contrast to simulations where activation above the cloud base is artificially suppressed.

Small cloud droplets (with radii $\lesssim 15\,\mu$m) grow efficiently by the diffusion and condensation of water vapour. Although at the droplet scale this is a complex process (see section 4.1 below), at the cloud scale the process can be significantly simplified. The growth of a single droplet can be described by (Mason, 1971, p. 123)

$$\frac{\mathrm{d}a}{\mathrm{d}t} = \gamma \frac{s}{a}, \tag{2}$$

where a is the droplet radius, $s = e/e_s - 1$ is the supersaturation (the excess water vapour with respect to saturation), e and e_s are respectively the actual and saturated vapour pressure and γ is a function of the ambient temperature and pressure (Rogers and Yau, 1989, p. 102). Equation (2) applies when a is larger than a few microns such that Raoult (solute), Kelvin (curvature) and kinetic effects can all be neglected. Since the rate of droplet growth is inversely proportional to its radius, small droplets grow faster than large droplets (when growth is considered in terms of droplet diameter; it would not be true if growth were considered in terms of droplet mass). Thus (2) predicts that the droplet size distribution becomes narrower as the mean droplet radius increases. Equation (2) also describes the evaporation of a droplet when s is negative (the saturation deficit). If s is assumed to be constant, (2) can be integrated to give a time scale, τ_e, for the evaporation of a droplet.

The supersaturation can be related to the vertical velocity, w, by (Squires, 1952; Twomey, 1959)

$$\frac{\mathrm{d}s}{\mathrm{d}t} = Aw - \frac{s}{\tau_s}, \tag{3}$$

where A is a thermodynamic variable which depends on the ambient temperature and τ_s is the phase relaxation time (the time-scale for s to approach equilibrium). This time-scale is related to the droplet number concentration and the mean droplet radius via $\tau_s \propto (n\overline{a})^{-1}$, where $\overline{a}$ is assumed to be constant (e.g. Politovich and Cooper, 1988; Korolev and Mazin, 2003; Kostinski, 2009). Typical values of τ_s vary from 0.23 s for $n = 1000$ cm^{-3} and $\overline{a} = 10$ μm to 14.1 s for $n = 100$ cm^{-3} and $\overline{a} = 2$ μm (Politovich and Cooper, 1988). The time-scales τ_s and τ_e can vary quite significantly depending on the choice of parameters. Indeed, Lehmann *et al.* (2009) show that even when τ_s and τ_e are comparable, the numerical solution of (2) and (3) (with no assumption of constant a or constant s) can yield a time-scale for droplet evaporation (or for s to reach equilibrium) that is

substantially different from either τ_s or τ_e. The first term on the right-hand side of (3) represents the increase in s due to adiabatic cooling in ascent and the second term represents the decrease in s due to the condensation of water vapour on droplets. The second term accounts both for the removal of water vapour from the ambient phase by the droplet and the change in s that occurs as a result of latent heat release. For $t \gg \tau_s$, the quasi-equilibrium supersaturation, $s_{\mathrm{qe}} = Aw\tau_s$, follows automatically from (3) for constant w and A. Since typical updraught velocities are approximately 1–5 m s^{-1}, then for the values of τ_s quoted above one would only expect significant deviations from s_{qe} for eddies smaller than at most a few tens of metres. For larger eddies, s will be close to s_{qe} for most of the time. Neglect of the second term on the right-hand side of (3) in some studies (see section 4.1.3 below) can lead to an unrealistic growth of s as then s_{qe} no longer imposes a constraint on s for large eddies.

The simple model of droplet growth provided by (2) and (3) is a reasonable approximation of reality (at least in the quasi-adiabatic cloud core with no mixing of entrained dry air) because the supersaturation rarely exceeds 0.1% (see, for example, Politovich and Cooper, 1988; Korolev and Mazin, 2003) except where the activated droplets have not grown enough to deplete it. As discussed above, CCN activation is generally confined to the first 100 m above cloud base except in vigorous convective clouds with vertical velocities of order 10 m s^{-1}, where the supersaturation can reach levels higher than 1% (Prabha *et al.*, 2011). This means that the total volume fraction of droplets in a cloud volume is generally equal to the difference between the total water mixing ratio and the saturation water vapour mixing ratio at the temperature of that cloud volume to within 1% or less. Both the total water mixing ratio and the enthalpy are conserved variables that do not depend significantly on microscale processes. This prediction of the macroscale theory is well supported by observations. For example, in stratocumulus clouds, the liquid water mixing ratio is close to adiabatic, except when approaching the cloud top (see Figure 3 in Pawlowska *et al.*, 2000).

3.2. Observations of cloud droplets

Some of the first observations with scattering spectrometers showed much broader size distributions in the quasi-adiabatic cloud core than predicted by (2). These observations triggered numerous studies for identifying physical processes that could explain this broadening. However, the instrument used to make these observations, the FSSP-100 (Forward Scattering Spectrometer Probe), had a poor size resolution (15 size classes to cover the range from 2 to 45 μm). Measurements with an improved version, the Fast-FSSP with 256 size classes (Brenguier *et al.*, 1998), revealed narrower spectra (in quasi-adiabatic cloud volumes) than previously observed (though not as narrow as predicted by (2)) well above cloud base in cumulus clouds (Brenguier and Chaumat, 2001). Since then the standard instrument has been significantly improved, with up to 40 size classes and observations of narrow spectra (typically with a standard deviation of 0.1 times the mean droplet radius; Brenguier *et al.*, 1998) are now more common. Observations of spectra as narrow as those predicted by (2), though, are not yet feasible with forward scattering particle counters because the relationship between droplet radius and the intensity of Mie scattering is not monotonic (see Figure 16 in Dye and

Baumgardner, 1984). Moreover, even if the instrument were perfect, the probability of finding a cloud volume that has not been affected by entrainment and mixing 1 km above cloud base is extremely low in real clouds. These limitations notwithstanding, LES of realistic clouds do a reasonable job of reproducing the main features of the droplet spectrum such as the effective radius of the droplets (defined as the ratio of the third moment of the droplet size distribution to its second moment) and the number concentration (see, for example, Jiang *et al.*, 2008; van Zanten *et al.*, 2011). However, the positive tail of the droplet size distribution, which accounts for the largest droplets, is poorly measured with single-particle counters, while it plays a crucial role in the onset of precipitation. Small-scale turbulence may therefore be important if it affects the proportion of the largest droplets that initiate precipitation but this is unlikely to be detected with existing single-particle counters. There is, however, some indirect evidence for spectral broadening: *in situ* measurements and satellite retrievals of stratocumulus show that it can start precipitating when the mean droplet radius reaches values larger than 12 µm (Gerber, 1996; Boers *et al.*, 1998; Pawlowska and Brenguier, 2003), while collision–coalescence requires droplets larger than 30 µm. This common observation thus suggests that droplet spectra with a mode around 12 µm also contain a significant fraction of droplets larger than 30 µm.

In the absence of turbulence, the spatial distribution of droplets would be random, with no correlation between the droplets. However, it is known from numerical simulations and laboratory experiments (see, respectively, sections 4.2.2.2 and 4.2.6 below) that the positions of droplets in turbulent flows are correlated over certain scales. The Fast-FSSP has been used to detect droplet clustering in real clouds: the aim is to distinguish clustering that occurs due to inertial-range mixing between cloudy filaments and cloud-free air (due to entrainment) from that which occurs at dissipation-range scales. The FSSP measures droplets along a narrow almost 1-D horizontal path through a cloud volume, which means that a long sample is necessary to construct a reasonable spectrum. The interpretation of the results remains controversial because deviations from Poisson distributions are always possible due to instrumental artefacts and the necessarily limited samples that are obtained from aircraft measurements, which inevitably compromise the assumption of the statistical homogeneity of the sample. Nevertheless, droplet counts in cumulus clouds have been analysed to quantify the departure from a Poisson distribution. A number of techniques have been developed to quantify this departure, including the Fishing test (Baker, 1992), clustering index (Chaumat and Brenguier, 2001), pair-correlation function and its volume average (Kostinski and Shaw, 2001; Shaw *et al.*, 2002; Lehmann *et al.*, 2007), analysis of power spectra (Pinsky and Khain, 2001, 2003) and analysis of correlations (Jaczewski and Malinowski, 2005). Mathematically, these techniques are related to each other (Shaw *et al.*, 2002; Baker and Lawson, 2010) but there remains some debate over the merits of each test when applied to real data. What is important is to assess the significance of any observed deviations from Poisson distributions against those produced by models. In this respect, and to mitigate the impact of instrumental artefacts, it is suggested that a stronger test is to compare observations with simulated droplet fields that are virtually sampled

using a simulator of the probe (as was done for two cases by Chaumat and Brenguier, 2001).

Shaw *et al.* (1999) argue that the difficulty of detecting spatial inhomogeneities in the droplet concentration may be related to the volume fraction associated with these inhomogeneities. Drawing on a model of fine-scale structure in turbulence by Tennekes (1968), which predicts that the volume fraction occupied by vortex tubes decreases with increasing R_λ, Shaw *et al.* (1999) hypothesize that the departure from Poisson statistics may be small because the volume fraction of vortex tubes is small and hence any localized clustering is likely to be masked by instrumental averaging. However, airborne samples are never perfectly homogeneous in the statistical sense and so inhomogeneities or deviations from a Poisson distribution will always be noticeable in airborne observations of real clouds. It is the impact of such deviations that is important but difficult to quantify, particularly with no information on the time-scale of these deviations.

4. Small-scale turbulence and cloud microphysics

In this section we consider the effect of small-scale turbulence on the growth of cloud droplets (though not in isolation from the large scales). In section 4.1 we consider its effect on condensational growth. Droplet growth by gravitational collision-coalescence only becomes efficient once a certain fraction of droplets reaches 30–50 µm in radius (Pruppacher and Klett, 1997, sections 14.5, 15.1–15.3; Xue *et al.*, 2008; Wang and Grabowski, 2009; Grabowski and Wang, 2009). The rapid growth of droplets from 15 to 50 µm remains difficult to explain. Indeed, 'rapid' remains poorly defined largely because of the lack of observations: it is difficult to measure this time interval since clouds only become visible to radar after drizzle-sized drops have already formed. Moreover, it will vary from one cloud type to another and will depend on the supersaturation and the liquid water content. Nevertheless, turbulence has long been considered to play an important role and this is discussed in section 4.2.

We defer discussion of the impact of entrainment and mixing on the droplet size distribution to section 5; this section may be regarded as appropriate for the quasi-adiabatic cloud core (at least in the early development of the cloud). Since our main interest is on cloud droplets less than 100 µm in radius, we shall assume that the droplets are spherical and ignore any deformation of droplets in close proximity to each other that may occur in reality. Similarly, we will not consider the fluid flow within the droplets. These have been discussed extensively in Pruppacher and Klett (1997, section 10.3) and are of secondary importance for most cases of interest.

A cloud droplet has a characteristic inertial response time, τ_p, which depends on its density, ρ_w, and radius, a. For small cloud droplets the Reynolds number based on the velocity of the droplet relative to the flow and the droplet diameter is usually assumed to be sufficiently small that Stokes drag can be used to good approximation. In this case, it can be shown (e.g. Batchelor, 1967, p. 234) that, since $\rho_w \gg \rho_a$, $\tau_p = 2\rho_w a^2/9\mu$, where μ is the dynamic viscosity of air. When there is no motion in the fluid, the particle equation of motion can be integrated to give an expression for the droplet velocity, v_p, at time t assuming zero initial velocity: $v_{p(t)} = v_T(1 - \exp(-t/\tau_p))$, where $v_T = \tau_p g$ is the (Stokes)

terminal velocity of the droplet and g is the acceleration due to gravity. While Stokes drag is appropriate for droplets less than 30 μm in radius, for larger droplets a nonlinear drag must be assumed since the droplet Reynolds number is $O(1)$. A parametrization due to Beard (1976) includes Reynolds number effects and has been successfully used in cloud simulations. The effect of a nonlinear drag on droplet collisions and growth is discussed in section 4.2.2. Most studies of droplets in turbulent fluids assume that the motion of the droplet is entirely governed by a drag force and gravity. In reality, though, there are a number of other forces that act on the droplet which are usually neglected since $\rho_w \gg \rho_a$ and on the assumption that fluid accelerations are much less than the gravitational acceleration (Maxey and Riley, 1983; Shaw, 2003). However, as discussed in Shaw (2003) and Siebert *et al.* (2010b), recent experimental and numerical research has shown that accelerations much larger than g are possible in localized regions of the flow (although such measurements have yet to be made in real clouds); the implications of this for cloud physics are not yet clear but the collision rate may well be sensitive to large but rare events.

For a typical small cumulus cloud the Kolmogorov length scale $\eta \approx 1000$ μm (e.g. Shaw, 2003), which is comparable with the typical inter-droplet distance (Pruppacher and Klett, 1997, p. 28). Since cloud droplets have radii much less than η, it is the dynamics of small-scale turbulence (in particular the dissipation range) which are important. However, it should be noted that large-scale flow features alter the background conditions seen by individual droplets and also impact on fine-scale intermittency, which increases with increasing L/η, where L is the integral scale of turbulence. The response of the droplet to changes in turbulence is characterized by the Stokes number, which is defined as St $= \tau_p/\tau_\eta$, where τ_η is the Kolmogorov time-scale. Since $\tau_\eta = (\nu/\varepsilon)^{1/2}$, where ν is the kinematic viscosity of air, it follows that St $\sim \varepsilon^{1/2}$.

Droplets falling under gravity have a mean velocity relative to the turbulent flow and hence the interaction time between the sedimenting droplets and the turbulent eddies will be reduced. The relative importance of turbulence and sedimentation may be quantified in terms of the dimensionless parameter Sv (Wang and Maxey, 1993; Vaillancourt and Yau, 2000). It is defined as the ratio of the eddy turnover time to the time taken for a droplet to sediment across that eddy, τ_v. For an eddy of order η, Sv $= \tau_\eta/\tau_v$, which can also be expressed as Sv $= v_T/v_\eta$, where v_η is the Kolmogorov velocity scale and noting that $\tau_v = \eta/v_T$. Since $v_\eta = (\varepsilon\nu)^{1/4}$, it follows that Sv $\sim \varepsilon^{-1/4}$. The ratio St/Sv $= (v_\eta/\tau_\eta)/g = v_\eta^2/(g\eta) = $ Fr$_f$ is independent of τ_p and is equal to the Froude number for the fluid, Fr$_f$.

As stated in the Introduction, many earlier DNS studies on turbulence–inertial particle interactions tend to have larger values of ε than is typical of clouds and hence may stress the importance of St instead of Sv (Grabowski and Vaillancourt, 1999). They are not designed for cloud droplets but are relevant to engineering applications where the dissipation rate may be several orders of magnitude higher. For typical cloud conditions ($\varepsilon \sim 100$ cm^2 s^{-3}, $\nu \sim 0.15$ cm^2 s^{-1}) and droplets of radius 15 μm, we have St ~ 0.07 and Sv ~ 1.4, indicating that gravity has a greater effect (compared with turbulence) on the collision rate of cloud droplets within dissipative eddies through its effect on the relative motion
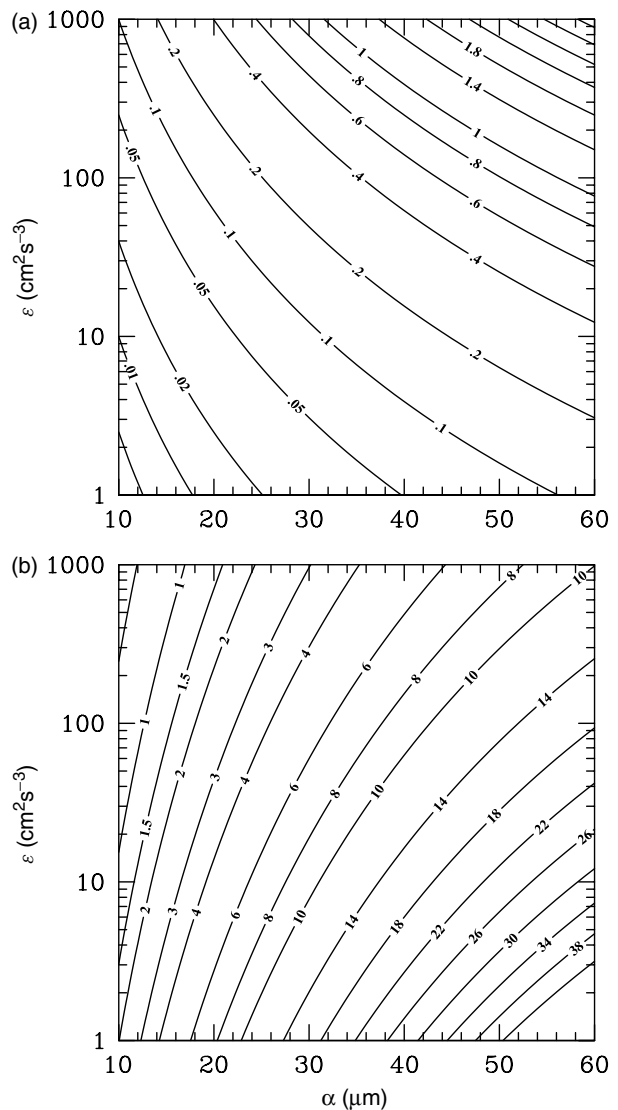
Figure 1. Contour plots of (a) Stokes number (St) and (b) non-dimensional terminal velocity (Sv) as a function of flow dissipation rate (ε) and droplet radius (a) (Ayala *et al.*, 2008a).

of cloud droplets and on the collision efficiency. Figure 1 shows the variation of St and Sv with droplet size and ε (for values relevant to cloud droplets) and indicates that typically St is less than one and Sv is greater than one. It is important to note, however, that even for the size range shown (10–60 μm) both parameters can vary by more than an order of magnitude. For small ε and larger droplet size (the lower right quadrant in Figure 1), gravity dominates the motion of droplets and turbulence only introduces a weak modification to the motion; thus the effect of inertial clustering is very weak. On the other hand, for small cloud droplets in regions of very large ε (the upper left quadrant in Figure 1) e.g. during the initial cloud droplet growth in actively convective clouds, St could be 0.1 or higher, while Sv is of order one or less. In this case, St could become an important parameter for quantifying phenomena such as the effect of clustering on the collision rate of cloud droplets. Numerical, theoretical and experimental studies (e.g. Ayala *et al.*, 2008a, 2008b; Lu *et al.*, 2010) have revealed that both parameters and their physical implications need to be carefully considered together in quantifying the pair interaction and collision of cloud droplets.

The above arguments rely on the variation of St and Sv with the mean dissipation rate. In reality, the dissipation rate has a distribution of values whose width increases with increasing R_λ. Fluctuations in the dissipation rate may well produce localized regions of the flow where St and Sv depart significantly from their values based on the mean dissipation rate. Moreover, the frequency of these regions and the intensity of the dissipation rate are likely to increase with increasing R_λ. This in turn could have a localized impact on processes which are very sensitive to turbulence such as droplet clustering. Of course, these regions may form only a very small fraction of the flow which, along with the non-stationarity of the flow, may render their overall effect negligible. However, it is possible that even if only a very small proportion of droplets are affected by localized regions of intense turbulence–the one-in-a-million lucky droplet that goes on to form rain (Kostinski and Shaw, 2005)–this could have a significant impact on precipitation. Recent analysis of droplets in 2-D turbulence (Dallas and Vassilicos, 2011) supports these arguments but demonstrates that they do not necessarily depend on small-scale intermittency (since the velocity-gradient statistics in 2-D turbulence are approximately Gaussian) or on differential gravitational settling (assuming a sufficiently large volume fraction).

4.1. Condensational growth and turbulence

Condensation in atmospheric clouds refers to the activation and growth of micron-sized droplets that takes place if the physical and thermodynamic conditions allow (pressure, temperature, water content in air). Since growth by diffusion of water vapour concerns cloud droplets with radii larger than a few tenths of a micron, the corresponding Knudsen number, defined by $\mathrm{Kn} = l_m/a$, with l_m denoting the molecular mean free path length of the air–vapour mixture (approximately 0.06 μm, so that $\mathrm{Kn} \sim 0.5$ for $a = 0.1\,\mu$m), is relatively low (but not very small, which is why non-continuum corrections are sometimes applied for $a < 1$ μm; e.g. Jennings, 1988). Therefore, a continuum approach can be used in modelling the exchange of water vapour and heat between the droplet and the ambient phase. A rigorous treatment of droplet growth by condensation involves the energy and mass balance of the fluid both inside and outside the droplet, subject to appropriate boundary conditions on the surface of all the droplets as well as in the far field of the ambient phase. For many droplets in constant motion, this direct approach is clearly not feasible for numerical computation and simplifications to the governing equations are therefore required. We start with a scale analysis of condensational growth (see also Vaillancourt et al., 2001), which provides the motivation for the simplifications to come.

4.1.1. Length scales associated with condensational growth of droplets

The condensational growth of droplets is characterized by vapour pressure gradients in the ambient phase and temperature gradients both inside and outside the droplet. We consider first the length scales associated with spatial variations in the ambient phase. In the classical theory of droplet growth by water vapour diffusion (e.g. Sedunov, 1974, p. 10; Pruppacher and Klett, 1997, section 13.2),

ambient conditions are defined by prescribed temperature and moisture fields far from an isolated droplet. Although the classical theory imposes these conditions at infinity, imposing them at a radius similar to the mean distance between droplets does not result in significant modifications (Fukuta, 1992). However, when the growth of an ensemble of droplets in turbulent air is considered, the temperature and the moisture fields away from the droplet may vary considerably and the concept of ambient conditions becomes vague. The 'boundary conditions' imposed between droplets now depend on both the spatial distribution of droplets as well as on the supersaturation and temperature fields. Following Vaillancourt et al. (2001) we define the ambient conditions to be the moisture and temperature fields in the vicinity of a given droplet averaged over the volume defined by the mean distance between droplets. This simplification is frequently applied in numerical models of droplet condensation in turbulence which employ the so-called point-particle approach to describe the evolution of the droplet phase (e.g. Vaillancourt et al., 2002; Celani et al., 2007; Lanotte et al. 2009).

Most studies of the growth of an ensemble of droplets in cloud physics neglect the direct interaction between droplets. The conventional justification (e.g. Sedunov, 1974, p. 133) is based on the argument that the mean distance between cloud droplets (~ 2 mm for a typical concentration of 100 cm^{-3}) is at least an order of magnitude larger than the distance ($\sim 10a$ or less) affected by the variation of moisture and temperature due to cloud droplet growth. Thus the volume of air occupied by a single cloud droplet is much larger than the volume affected by variations in the moisture and temperature. Although some authors (Sedunov, 1974; Fukuta, 1992) have concluded that direct competition between droplets is negligible under typical cloud conditions, there is yet to be a clear demonstration that these effects are not important.

4.1.2. Time-scales associated with condensational growth of droplets

There are a number of time-scales associated with the condensational growth of cloud droplets. The first is associated with the diffusional growth of an isolated droplet. During this process water vapour is transported from the environment to the droplet surface by molecular diffusion and by convective transport (the *ventilation effect*, which accounts for the motion of the droplet; e.g. Rogers and Yau, 1989, p. 116). Latent heat released at the droplet surface is transported both to the environment and inside the liquid droplet by the same mechanisms. These processes can be calculated explicitly by solving a set of three convection–diffusion equations for water vapour, heat outside the droplet and heat inside the droplet. Sedunov (1974, p. 13) showed that, under typical atmospheric conditions, the convective transport can be neglected when considering the condensational growth of droplets with radii smaller than 30 μm, which means that only diffusive transport needs to be accounted for.

By considering the diffusion of water vapour and heat on to or inside a still droplet (with constant surface temperature), Sedunov (1974, p. 18) obtained three characteristic time-scales for the approach to a steady state for these processes. They are $\tau_q = a^2/\pi K_v$, $\tau_{\mathrm{Ti}} = a^2/\pi K_w$, $\tau_{\mathrm{To}} = a^2/\pi K_a$ for respectively the diffusion of water vapour,

temperature inside and outside the droplet, where K_v is the diffusivity of water vapour and K_a, K_w are respectively the thermal diffusivities of air and liquid water. The slowest of the three time-scales is τ_{Ti} which typically varies from 6×10^{-5} s for $a = 5$ μm to 1×10^{-3} s for $a = 25$ μm (Vaillancourt *et al.*, 2001). In comparison, the flux of water vapour or heat in air to or from the droplet will approach its steady-state value within a few microseconds, meaning that for an isolated droplet the conditions in the ambient phase (i.e. vapour pressure and temperature) will relax much faster to their steady-state values (than occurs within the droplet).

Another time-scale occurs when the boundary conditions for water vapour concentration and temperature at the surface of the droplet are not assumed to be constant. During condensation water vapour diffuses on to the surface of the droplet, latent heat is released and consequently the surface temperature (the *psychrometric temperature*) of the droplet changes. The relaxation time associated with this last process lies typically between 5×10^{-4} s and 1×10^{-2} s for droplet radii between 5 and 25 μm (Vaillancourt *et al.*, 2001) and is therefore the slowest time-scale associated with the condensational growth of a droplet. Vaillancourt *et al.* (2001) showed that, for $a \lesssim 20$ μm and $\varepsilon \lesssim 100$ cm^2 s^{-3}, the ratio of this time-scale to the fastest time-scale associated with changes to the ambient conditions due to turbulence (either τ_η or τ_v) is much less than one and hence that the assumption of a steady-state distribution of water vapour concentration and temperature is valid. This assumption becomes less valid for increasing a and ε, so that it may be necessary to take into account a time-varying psychrometric temperature for $a \gtrsim 20$ μm and $\varepsilon \gtrsim 200$ cm^2 s^{-3}. However, for such large cloud droplets, the condensational growth is generally slow compared with growth associated with collision–coalescence and the error due to the above quasi-equilibrium assumption becomes irrelevant.

4.1.3. Theoretical models and numerical simulations of condensational growth in a turbulent fluid

There has been much theoretical interest in what effect vertical velocity fluctuations and spatial inhomogeneities in the distribution of droplets have on the supersaturation field and the subsequent condensational growth of droplets (see, for example, Cooper, 1989; Srivastava, 1989; Khvorostyanov and Curry, 1999). Here, we consider some of these ideas and, in particular, the recent numerical simulations that have been constructed to test them.

The theory of stochastic condensation was developed to model the condensational growth of droplets in a turbulent fluid (e.g. Sedunov, 1974, p. 192). The stochastic condensation equation can be derived by Reynolds-averaging the part of (1) that pertains to condensational growth (e.g. Shaw, 2003). (Note that $f(a)$ is not strictly a probability density function (pdf) as it may evolve differently in each realization of the flow; an ensemble average of $f(a)$ would give a true pdf.) Assuming the air is locally incompressible, ignoring droplet inertia and any sources or sinks of droplets, the stochastic condensation equation is given by

$$\frac{\partial \overline{f}}{\partial t} + \overline{u}_i \frac{\partial \overline{f}}{\partial x_i} = -\frac{\partial (\overline{u_i' f'})}{\partial x_i} - \frac{\partial (\overline{a}\,\overline{f})}{\partial a} - \frac{\partial (\overline{a' f'})}{\partial a} \quad (4)$$

where an overbar represents a mean quantity and a prime indicates a fluctuating quantity. By analogy with reacting flows (e.g. Dimotakis, 2005) we introduce a Damköhler number, Da $= \tau_r/\tau_s$, where τ_r is the time-scale of a turbulent eddy of scale r. Equation (4) is usually solved in the *low-frequency* limit, Da $\gg 1$. In this limit, turbulent fluctuations are slow compared with thermodynamic changes to the droplet and it is then appropriate to assume that $s = s_{qe}$ (see the discussion following (3)). Reynolds-averaging of s_{qe} indicates that the mean and fluctuating parts of s_{qe} are directly related to the mean and fluctuating vertical velocity component respectively.

The following scale analysis shows that the low-frequency limit ceases to be valid for scales of several metres and smaller. Since $\tau_r \sim r^{2/3}/\varepsilon^{1/3}$, the scale at which Da ~ 1 is given by $r \sim (\varepsilon \tau_s^3)^{1/2}$ which, for typical cloud conditions, can be several metres (Shaw, 2003). Khvorostyanov and Curry (1999) considered the stochastic condensation equation for arbitrary values of τ_r and τ_s. They hypothesize that there are fluctuations of s at the droplet scale which do not depend directly on w' (but may be indirectly related to turbulent fluctuations via the distribution of droplets and the properties of the air in the vicinity of the droplets through the mixing of different air parcels). Khvorostyanov and Curry (1999) argue that, at small scales, s' should be proportional to a and not w'. They base their arguments on the supposition that larger droplets are more likely to benefit from an increase in s' at the expense of smaller droplets which cannot compete as effectively for the available water vapour. (This scenario is equivalent to the inhomogeneous mixing of dry and cloudy air discussed in section 5.1 below.) Additionally, by considering kinetic and curvature corrections to the water vapour diffusivity (see also Pruppacher and Klett, 1997, p. 506) they showed that $s'(a, t) \sim m(t)a$, where $m(t)$ has a slope that decreases with time. Thus these corrections become negligible at large times when the low-frequency solution of (4) is the appropriate solution. It is the suppressed growth of smaller droplets, which is inherent to their model, that facilitates broadening of the droplet spectrum.

Vaillancourt *et al.* (2001) showed that randomly distributed non-sedimenting droplets create significant perturbations in the supersaturation with spectral broadening dependent on the width of the initial size spectrum. When the droplets are allowed to sediment, the correlation time of the supersaturation perturbations is reduced and hence also the integral of the supersaturation and the consequent growth of the droplet spectrum. Vaillancourt *et al.* (2001) concluded that a static random distribution of droplets is insufficient to explain broadening of the droplet spectrum. Pinsky *et al.* (1999a) consider the effect of turbulence on the condensational growth rate by dividing a large cloud volume into centimetre-scale volumes each with its own droplet velocity flux divergence which is related to the lifetime of a centimetre-scale turbulent vortex. Pairs of centimetre-scale volumes exchange droplets, leading to inhomogeneities in the droplet concentration and differences in the supersaturation and droplet growth rates. Pinsky *et al.* (1999a) found that mimicking the effects of small-scale turbulence in this way leads to a modest increase in the broadening of the droplet spectrum. Shaw *et al.* (1998) consider the effect of droplet clustering on the condensational growth rate by using a Rankine vortex to model a typical turbulent eddy along with (2) and (3). They find that the droplet spectrum broadens with time with a sensitivity to the values

of ε and τ_s. Their model indicates that the production of large droplets and spectral broadening are optimal for $\varepsilon = 100\ \mathrm{cm}^2\,\mathrm{s}^{-3}$ and $\tau_s = 10\ \mathrm{s}$. Shaw *et al.* (1998) argue that turbulence-induced fluctuations in droplet concentration induce large fluctuations in s, which means that individual droplets grow at different rates depending on their location in the flow. These arguments were extended by Shaw (2000), who proposed a mechanism for the formation of bursts of very high supersaturation levels based on the interaction of droplets with rare but intense vortex tubes, which have been observed in turbulent flows and are thought to be related to fine-scale intermittency. This model suggests that in undiluted regions of a turbulent cloud (e.g. the core updraught of a cumulus cloud) the droplet size distribution should be close to the distribution expected for the simple macroscopic model described in section 3.1 but with an increased number of small droplets due to secondary activation of droplets in regions of high supersaturation and a small concentration of superadiabatic droplets which experience rapid growth in decaying vortex tubes. The studies of Shaw (2000) and Vaillancourt *et al.* (2001) are not necessarily contradictory since the latter assumes that droplet growth is determined by mean-field quantities and does not take account of intermittency effects; the importance of rare events in the condensational growth of droplets remains an open question.

Celani *et al.* (2005) considered condensational growth of non-sedimenting droplets in a numerical simulation of a turbulent velocity field by coupling an advection–diffusion equation for s with a forcing term identical to the first term on the right-hand side of (3), but without the second term, to the Navier–Stokes equations. The results of their 2-D simulation of turbulence showed a strong correlation between the droplets and supersaturation even when they included sedimentation in their model. This correlation means that each droplet experiences the same supersaturation for a long time (of the order of the large-eddy turnover time) and hence droplets in regions of high s grow faster than droplets in regions of low s, which leads to a broadening of the droplet size distribution. Celani *et al.* (2007) extended this model to a more realistic Boussinesq flow along with a term representing the depletion of water vapour due to condensation (i.e. the second term on the right-hand side of (3)) in the advection–diffusion equation for s (though with no sedimentation of droplets). They found that the spreading of the droplet spectrum and the mean droplet growth rate were reduced compared with their earlier simulations but were more realistic. As discussed in section 3.1, the absence of the second term on the right-hand side of (3) in simulations of condensational growth of droplets in a turbulent fluid can lead to unrealistically high values of s, which in turn can result in broader droplet size distributions and higher-than-observed liquid water content. This is particularly important at larger scales, as here s should approach s_{qe}.

Vaillancourt *et al.* (2002) were the first to study the condensational growth of droplets in 3-D DNS of homogeneous isotropic turbulence (for R_λ ranging from 12 to 34). In contrast to Celani *et al.* (2005), they found that sedimentation significantly reduces the broadening of the droplet spectrum; the reasons for this difference are not clear but could be related to the dimensionality of the simulations, the forcing of the flow or different parts of the St–Sv parameter space. Vaillancourt *et al.* (2002) also found that increasing ε leads to an increase in the instantaneous

standard deviation of the supersaturation fluctuations, which the authors attribute to increased droplet clustering. However, this does not compensate for a steadily decreasing correlation time between the supersaturation fluctuations and the droplets as ε increases. The result is that the width of the droplet size distribution, which is a function of the integrated supersaturation fluctuations along each droplet trajectory, decreases with increasing ε. They concluded that small-scale turbulence alone does not produce significant spectral broadening. As the discussion here and in the previous paragraph suggests, there remains some dispute over the importance of gravity in the study of droplets with radii less than 20 μm, with some authors arguing that sedimentation substantially reduces the supersaturation perturbations and consequently the width of the droplet size distribution (Vaillancourt *et al.*, 2001, 2002), while others argue that it is not significant (see the discussion in Grabowski and Vaillancourt, 1999, and Shaw *et al.*, 1999).

Lanotte *et al.* (2009) also considered the condensational growth of droplets in 3-D DNS (for R_λ ranging from 40 to 185). Their results show that the standard deviation of the squared droplet radius, σ_{a^2}, grows linearly with the large-eddy turnover time (for approximately constant ε), from which they argued that $\sigma_{a^2} \sim R_\lambda^{5/2}$. This scaling assumes that the standard deviation of the supersaturation, σ_s, does not deviate significantly from its initial value. At Reynolds numbers typical of real clouds, for which the large-eddy turnover time will be much larger than in the DNS of Lanotte *et al.* (2009), this assumption may no longer hold. Lanotte *et al.* (2009) argue that a more appropriate scaling follows from assuming that σ_s takes its equilibrium value. This leads to $\sigma_{a^2} \sim R_\lambda^{3/2}$. These two scalings then represent respectively lower and upper bounds on the Reynolds number dependence of σ_{a^2}. Lanotte *et al.* (2009) test their hypothesis by conducting a quasi-LES (DNS that matches typical large-scale cloud parameters but with unrealistic small scales such as η and τ_η) so that the large-eddy turnover time is now much larger than τ_s and s tends to s_{qe}. They find that, at large times, σ_{a^2} is close to its lower bound.

Sidin *et al.* (2009) studied condensational growth using kinematic simulation. Rather than solving the Navier–Stokes equations, a turbulent-like velocity field with an appropriate spectrum is constructed from a linear superposition of independent random Fourier modes (e.g. Fung *et al.*, 1992). Compared with DNS, kinematic simulation is computationally inexpensive and so a much wider range of scales is possible. Thus it may provide valuable insight into the combined effects of large and small scales. However, because the velocity field is synthesized rather than derived from the Navier–Stokes equations, it may not give the correct quantitative behaviour. Sidin *et al.* (2009) considered two models of condensational growth: a two-way coupled model which includes the effect of latent heating and water vapour depletion and a simplified model in which there is no two-way coupling. The simplified model shows a broadening of the droplet size distribution and the more realistic two-way coupled model also shows broadening but much less so than the simplified model, though still broader than the classical case of no turbulent mixing (i.e. latent heating and vapour depletion alone). By examining the broadening as a function of wave number, they argued that both large and small-scale turbulence are required to achieve spectral broadening within a control volume comparable with the smallest scales

of turbulence: the large scales transport droplets through regions of different supersaturations whereas the small scales mix droplets of different sizes. (Note that for a large control volume an unrealistically broad spectrum may be achieved with no mixing, since those droplets that experience high values of s grow faster than they would otherwise if mixing were to move them to regions of low values of s; mixing can also limit spectral broadening over large volumes.) They found that simulations with either large or small scales alone did not produce spectral broadening in a control volume of the same size. Large-scale effects are associated with droplets growing at different rates in different eddies; s_{qe} may vary from one large-scale eddy to another since each eddy may have a different vertical velocity. As postulated by Cooper (1989), the width of the droplet spectrum depends on the history of each droplet as it moves from one large-scale eddy to another, *large-scale eddy hopping*, and it is the small scales that allow a droplet to move in this way. The coexistence of differently sized droplets in a small volume is likely to be important for determining the collisional growth rate.

4.2.   Collisions, coalescence and turbulence

The collision and coalescence of droplets in a turbulent flow are governed by (i) geometric collisions due to the effect of turbulence on the droplets; (ii) collision efficiency due to droplet-droplet interactions; and (iii) coalescence efficiency due to droplet surface properties.

In practice, it is difficult to distinguish experimentally between collision and coalescence and the preferred experimentally measurable quantity is the *collection efficiency*. This is defined in the absence of turbulence to be the ratio of the actual coalescence cross-section, πx_c^2, where x_c is the critical value of the horizontal distance between the two droplets below which coalescence is certain to occur, to the geometric cross-section, πr_c^2, where $r_c = a_1 + a_2$ is the collision radius for two droplets with radii a_1 and a_2 (Pruppacher and Klett, 1997, p. 591; Rogers and Yau, 1989, p. 126). If coalescence is assumed to follow whenever $x_c < r_c$, then the collection efficiency is equal to the collision efficiency (i.e. we can neglect (iii) above). Vohl *et al.* (1999) have conducted wind tunnel experiments which show that this is approximately the case for $a < 100\,\mu$m (although the experiments were performed at lower Reynolds numbers than are typical of the atmosphere). Droplet growth through collection thus reduces to a problem of determining collision rates.

Collisions that result from the finite size of the droplets (neglecting the disturbance flows due to droplets) are known as *geometric collisions* and are considered in section 4.2.2. Geometric collisions do not necessarily result in coalescence between droplets; coalescence arises from interactions between droplets as a result of the perturbed flow field induced by one droplet in the vicinity of another. Such interactions are often referred to as hydrodynamic or aerodynamic droplet interactions and are considered in section 4.2.4. Droplet–droplet interactions determine the collision efficiency. In the absence of turbulence, gravity-induced collision efficiencies for cloud droplets tend to be in the range 0.001–0.1 (Pruppacher and Klett, 1997, p. 582).

4.2.1.   The collision kernel

We consider collisions of a bidisperse suspension of droplets in a turbulent flow. The average collision rate per unit volume, $\langle \mathcal{N}_{12} \rangle$, can be expressed as

$$\langle \mathcal{N}_{12} \rangle = \langle n_1 \rangle \langle n_2 \rangle \Gamma_{12}, \tag{5}$$

where $\langle n_1 \rangle$ and $\langle n_2 \rangle$ are the average number densities (per unit volume) of droplets with radii a_1 and a_2 respectively. In the monodisperse case, the right-hand side of (5) would have a factor of 1/2 for $\langle n \rangle \gg 1$. Note that the average collision rate per unit volume may be very different from the instantaneous collision rate since $\langle n_1 n_2 \rangle \neq \langle n_1 \rangle \langle n_2 \rangle$.

In the case of sedimenting droplets in stagnant air, the collision kernel becomes (Rogers and Yau, 1989, p. 130)

$$\Gamma_{12} = \pi r_c^2 |v_{T2} - v_{T1}|, \tag{6}$$

where v_{T1}, v_{T2} are respectively the terminal velocities of the two droplets. For spherical droplets that are much smaller than η and follow a turbulent flow exactly (i.e. with no inertia), Saffman and Turner (1956) showed that the collision kernel can be expressed as

$$\Gamma_{12} = r_c^3 \left(\frac{8\pi\varepsilon}{15\nu} \right)^{1/2}. \tag{7}$$

This represents the effect on the collision rate of the local shear at the dissipation (Kolmogorov) scale. The collision kernel can be generalized to the case where the finite inertia of the droplets becomes important (but not so much so that they are insensitive to changes in the turbulent flow).

More generally, Γ_{12} can be defined as the volume influx containing droplets of radius a_2 to a droplet of radius a_1 over the collision surface S_c about the centre of droplets of radius a_1 and radius r_c. For spherical droplets $\langle \mathcal{N}_{12} \rangle$ is given by (Sundaram and Collins, 1997; Wang *et al.*, 1998a, 2000; Ayala *et al.*, 2008b)

$$
\begin{aligned}
\langle \mathcal{N}_{12} \rangle &= 4\pi r_c^2 \langle n_1(a_1) n_2(a_1 + r_c) (-w_{12})|_{w_{12}<0} \rangle \\
&\approx 4\pi r_c^2 \frac{1}{2} \langle n_1(a_1) n_2(a_1 + r_c) |w_{12}| \rangle \\
&\approx 2\pi r_c^2 \langle n_1(a_1) n_2(a_1 + r_c) \rangle \overline{|w_{12}|} \\
&\approx 2\pi r_c^2 \langle n_1 \rangle \langle n_2 \rangle g_{12}(r_c) \overline{|w_{12}|}, \tag{8}
\end{aligned}
$$

where

$$g_{12}(r_c) = \frac{\langle n_1(a_1) n_2(a_1 + r_c) \rangle}{\langle n_1 \rangle \langle n_2 \rangle}$$

is the radial distribution function (RDF) and

$$\overline{|w_{12}|} = \frac{\langle n_1 n_2 |w_{12}| \rangle}{\langle n_1 n_2 \rangle}$$

is the density-weighted longitudinal relative velocity between droplets (evaluated at the collision radius r_c). The general collision kernel is then

$$\Gamma_{12} = 2\pi r_c^2 g_{12}(r_c) \overline{|w_{12}|}. \tag{9}$$

In deriving (8) we have assumed that half the particles are moving towards the surface as moving away, i.e. the

droplet surface is perfectly reflecting. This is equivalent to assuming that, when the surface is perfectly absorbing, the concentration falls by one half over a short distance of order the particle stop distance, which is infinitesimally small for a passive tracer (see Figures 14–16 in Ammar and Reeks, 2009). If the droplets were passive tracers, they could only coalesce by virtue of interception, which would mean that $g_{12}(r_c) < 1$ for small r_c. In reality, the influence of inertia would alter this picture since droplets can coalesce by inertial projection onto the collision surface or what is known in turbulent deposition models as *free flight to the wall* (see section 4.2.5).

The discussion in the preceding paragraph illustrates the effect of the boundary conditions on the collision rate: perfect absorption (coalescence) can be significantly different from perfect reflection (no coalescence). In their classic study of collision rates, Saffman and Turner (1956) (see (10) below and attendant discussion) assumed that the collision rate is the same whether the surface is perfectly absorbing or reflecting. However, several studies (e.g. Sundaram and Collins, 1997; Wang *et al.*, 1998b; Chun *et al.*, 2005; Ammar and Reeks, 2009) have shown that this is not the case. The persistence or finite lifetime of turbulent structures can make droplet collision rates very much rate-limited by diffusion in the vicinity of the droplets, as is the case of particle transport in a turbulent boundary layer. For geometric collisions, there are no boundary conditions since the motion of each droplet is treated as being independent of all the other droplets, collisions occurring when the sum of the radii of two droplets equals the collision radius.

4.2.2. Geometric collisions

DNS results (Pinsky *et al.*, 2006; Franklin *et al.*, 2007; Ayala *et al.*, 2008a) show that turbulence can increase the collision kernel relative to the case of stagnant air through increases in both the magnitude of the relative velocity and the RDF. The effect of turbulence on geometric collisions amounts to parametrizing these two effects: the droplet relative velocity and droplet clustering.

4.2.2.1. Droplet relative velocity

In bidisperse suspensions, $\overline{|w_{12}|}$ is always larger than its monodisperse counterpart: $\overline{|w_{12}|} \gg \max(\overline{|w_{11}|}, \overline{|w_{22}|})$ (Zhou *et al.*, 2001). This can be understood by considering first a monodisperse suspension, which represents a limiting case of the bidisperse suspension, in the absence of gravity. For low St, velocities of equally sized droplets are strongly correlated with the fluid (and so with each other), leading to low relative velocities. As St increases, the correlation of the droplets with the flow decreases and $\overline{|w_{11}|}$ increases. However, this increase is not unbounded since, for St $\gg 1$, droplets respond slowly to changes in the fluid velocity and hence $\overline{|w_{11}|}$ decreases. For bidisperse droplets, the velocities of the droplets decorrelate more rapidly than the equivalent monodisperse cases since droplets with different inertia respond differently to changes in the flow. The presence of gravity further increases the decorrelation of the droplets, leading to higher values of $\overline{|w_{12}|}$, as demonstrated in the DNS results of Woittiez *et al.* (2009).

Saffman and Turner (1956) were the first to obtain an analytical expression for $\overline{|w_{12}|}$ that combines the effects of droplet inertia and gravity:

$$\overline{|w_{12}(r_c)|} = \left(\frac{8}{3\pi}\right)^{1/2} \left[3(\tau_{p2} - \tau_{p1})^2 \overline{\left(\frac{D\boldsymbol{u}}{Dt}\right)^2} \right.$$
$$\left. + \frac{1}{3} r_c^2 \frac{\varepsilon}{\nu} + g^2 (\tau_{p2} - \tau_{p1})^2 \right]^{1/2}, \quad (10)$$

where τ_{p1}, τ_{p2} are respectively the characteristic response times of two droplets. The first term on the right-hand side of (10) represents the effect of fluid acceleration, the second term the local fluid shear and the third term the effect of gravity. Equation (10) was derived assuming that $\tau_p \ll \tau_\eta$ (where τ_p is typical of either droplet). Note that (10) does not account properly for gravity as it does not reduce to (6) (via (9)) in the absence of turbulence (for which $g_{12}(r_c) = 1$). Furthermore, when droplet inertia is neglected, (7) cannot be recovered from (10). These discrepancies arise from assuming that the effect of turbulence on the droplets is isotropic, which is reasonable in the absence of gravity but cannot be justified when gravity is included (Dodin and Elperin, 2002; Wang *et al.*, 1998a). These discrepancies can be corrected as shown in Wang *et al.* (2005c).

There have been many further attempts to derive improved analytical expressions for the droplet relative velocity (see, for example, Ayala *et al.* (2008b) or Xue *et al.* (2008) for a detailed review). Not surprisingly, the limiting cases of small and large droplet inertia, usually without gravity, have received more attention than cases with moderate inertia. When $\tau_p \lll \tau_\eta$, Ayala *et al.* (2008b) derived an analytical expression for sedimenting droplets which is partly based on the work by Dodin and Elperin (2002), who considered droplets with $\tau_p \ll \tau_\eta$.

The basic assumption of Ayala *et al.* (2008b) is that the droplet relative velocity is mostly determined by gravitational sedimentation and that droplet inertia introduces a secondary correction. This assumption is appropriate when the terminal velocity of droplets is large relative to the Kolmogorov velocity and works best when the two droplets are not close in size. Following Dodin and Elperin (2002) they decompose the droplet relative velocity into a deterministic part due to gravity, which follows from assuming Stokes drag, and a random part due to the turbulent fluctuations. Ayala *et al.* (2008b) assume that the random variable in this decomposition is normally distributed so that the problem of determining $\overline{|w_{12}|}$ reduces to that of determining the variance, σ_w^2, of the longitudinal relative velocity, for which they derive an analytical expression. In the limit $\tau_p \ll \tau_\eta$, their general expression for σ_w^2 becomes

$$\sigma_w^2 = (\tau_{p2} - \tau_{p1})^2 \overline{\left(\frac{D\boldsymbol{u}}{Dt}\right)^2} + \frac{1}{15} r_c^2 \frac{\varepsilon}{\nu}$$
$$+ (v_{T1}\tau_{p1} - v_{T2}\tau_{p2})^2 \frac{2\varepsilon}{15\nu}.$$

The first two terms on the right-hand side are similar to the first two terms on the right-hand side of (10). The third term is new and represents a coupling between gravity and the fluid shear. For typical cloud conditions, the ratio of this term to the shear term quickly becomes important as the size of the droplets increases. Ayala *et al.* (2008b) show that gravity appears to enhance the turbulent fluctuations (see Figure 7 of

Ayala *et al.*, 2008b) but reduces the variance of the individual droplet velocities and the droplet correlation coefficient (see Figures 8 and 9 respectively of Ayala *et al.*, 2008b).

Pinsky *et al.* (2006) consider the effects of non-Gaussian Lagrangian fluid accelerations on the collision kernel. They obtained lower values of Γ_{12} compared with the theoretically derived collision kernel of Wang *et al.* (1998a). They attribute this reduction to the assumption of normally distributed droplet relative velocities made by Wang *et al.* (1998a). Ayala *et al.* (2008b) find that the dependence of $\overline{|w_{12}|}$ on R_λ is weaker than that of Pinsky *et al.* (2006). They argue that the reason for this is that, because of sedimentation, the relative positions of the droplets are continuously changing and hence the fluid velocity experienced by each droplet within the pair is not necessarily perfectly correlated as was assumed by Pinsky *et al.* (2006). If the fluid velocity experienced by each droplet is perfectly correlated then the interaction between the two droplets occurs within the same fluid eddy and the lifetime of the interaction is not affected by sedimentation. By allowing for decorrelation between the fluid velocity experienced by each droplet, the coupling between the eddy–droplet interaction and sedimentation can be explicitly accounted for. Ayala *et al.* (2008b) argue that this results in a smaller enhancement of $\overline{|w_{12}|}$ compared with the perfectly correlated case (see Figure 14 in Ayala *et al.*, 2008b). When the two droplets in the pair are of similar size, so that differential sedimentation is no longer important, the model of Ayala *et al.* (2008b) underestimates $\overline{w}_{12}(r)$ compared with Pinsky *et al.* (2006).

As stated above, when nonlinear drag is assumed the terminal velocity is reduced compared with Stokes drag. This reduces the droplet relative velocity and the magnitude of the collision kernel for bidisperse droplets (Franklin *et al.*, 2007; Ayala *et al.*, 2008a). For monodisperse droplets larger than approximately 40 μm, Ayala *et al.* (2008a) found that nonlinear drag increases both $\overline{|w_{12}|}$ and the collision kernel.

A recent DNS study by Onishi *et al.* (2009) suggests that for monodisperse droplets gravity reduces collision frequencies for certain values of St and R_λ. They attribute this decrease to a decrease in the droplet relative velocity most likely because of the reduced interaction time between the droplet and the fluid eddies. These authors also derive a model from their DNS on the basis of which they argue that gravitational contributions to collisions can be neglected for monodispersed cloud droplets.

4.2.2.2. Droplet clustering

The field of droplets that is advected by the air may be regarded as a continuum (for *St* not too large). In the parlance of multiphase flows, the air is known as the *carrier flow field*. Even if the air is regarded as locally incompressible, the droplet continuum may be compressible. Maxey (1987), in his seminal work on settling in turbulent flows, was the first to relate particle clustering to the local divergence of the particle velocity field and gave an expression for it to first order in St, namely

$$\nabla \cdot \boldsymbol{v}_p(\boldsymbol{x}, t) \sim -\text{St}(S^2 - R^2), \qquad (11)$$

where $\boldsymbol{v}_p$ is here interpreted as the particle velocity field, **S** is the local symmetric rate of strain tensor of the carrier fluid and **R** is the local rotation tensor. In statistically stationary homogeneous isotropic incompressible flows $\langle S^2 \rangle_p - \langle R^2 \rangle_p = O(\text{St})$ for inertial particles, where $\langle \cdot \rangle_p$ indicates an ensemble average following a particle, and so $\left\langle \boldsymbol{\nabla} \cdot \boldsymbol{v}_p(\boldsymbol{x}, t) \right\rangle_p = -O(\text{St}^2)$. Equation (11) quantitatively embodies the now commonplace and appealing view first proposed by Maxey (1987) that inertial particles segregate into the straining regions in the flow between the regions of vorticity. The implication is that the net divergence along a particle trajectory is negative and clustering is not a statistically stationary process, so that the net concentration along a particle trajectory would continually increase in time. This small-St-number approximation for both the particle velocity field and its divergence has been the source of a number of analyses and simulations. In this regard, particularly important have been the analytical forms derived for the radial distribution function $g(r)$ and their power law dependence on r as $r \to 0$ (see below), which would indicate that $g(r) \to \infty$ as $r \to 0$. Numerous simulations of particle motion for small St in isotropic turbulence have led to confirmation of this long-term equilibrium form (e.g. Chun *et al.*, 2005; Kerstein and Krueger, 2006).* For details of how this equilibrium is approached and the need for an ever-increasing grid refinement to observe the RDF accurately as $r \to 0$ (since more particles are required to preserve statistical accuracy) the reader is referred to IJzermans *et al.* (2009). Insufficient resolution leads to an apparent equilibrium at a shorter time: in fact, for particles with a collision radius r_c the time for equilibrium $t_e/\tau_\eta \to \infty$ as $r_c/\eta \to 0$. This viewpoint of an approach to equilibrium as $t \to \infty$ is not incompatible with a net finite negative divergence (compressibility) which compresses an elemental volume of particles until they touch. Balkovsky *et al.* (2001) considered this limit, and also that imposed by Brownian motion, giving a lower bound to the clustering as the separation distance approaches $r_d \sim (D_B/S)^{1/2}$, where $S \sim \sqrt{\epsilon/\nu}$ and D_B is the Brownian diffusion coefficient, for which t_e is of order $\lambda_p^{-1} \ln(\eta/r_d)$, where λ_p is the typical value of the particle velocity field gradient. Thus the limiting value of the power law for the concentration depends on whether $r_c \leqslant r_d$.

Clustering of inertial particles has been extensively studied both experimentally (see section 4.2.6) and in numerical simulations (e.g. Sundaram and Collins, 1997; Reade and Collins, 2000) though with relatively few studies of sedimenting droplets. These studies indicated that particle clustering reaches a maximum for St ~ 1 and tends to zero (uniform mixing) as St $\to \infty$. They have also resulted in a number of empirical formulations for $g(r)$. For values of St not too large, the RDF for a monodisperse system typically takes the form of a power law which reflects the multi-scale self-similar nature of droplet clustering (e.g. Figures 7 and 8 of Goto and Vassilicos, 2006; Bec, 2005; Bec *et al.*, 2007). This multi-scale clustering has been accounted for in terms of the sweep-stick mechanism, which explains why droplet clustering mimics the multi-scale clustering of vanishing fluid acceleration points in a turbulent flow (Coleman and Vassilicos, 2009). Analytical expressions for the RDF have been derived by Chun *et al.* (2005) for St $\ll 1$ and Zaichik and Alipchenkov

---

*Note that in both these simulations the simulated particle velocity field is assumed to be zero. This neglects the component due to *random uncorrelated motion* (see section 4.2.5), which manifests itself as a mean drift velocity proportional to the gradient of the particle kinetic stresses (referred to as turbophoresis).

(2003) for values of St including St $\gtrsim$ 1. The latter was derived using pdf methods (analogous to kinetic theory) but does not give a closed-form expression for $g(r)$. In principle, this approach can be extended to cover the Abrahamson limit, St $\gg$ 1 (Abrahamson, 1975). There has, until recently, tended to be more interest in the limit St $\ll$ 1 than St $\gtrsim$ 1. Particularly useful in the study of the latter region has been the so-called fully Lagrangian method (Osiptsov, 2000) and a similar method implemented by Falkovich and Pumir (2004, 2007) and Ducasse and Pumir (2009). The application of either of these approaches means that as well as calculating the droplet velocity and position along a trajectory, one can also calculate the compressibility. This also enables one to calculate the particle concentration (the rate of change of which is proportional to the divergence of the particle velocity field) along a particle trajectory and in turn the statistical moments of the volume-averaged particle concentration. IJzermans *et al.* (2009, 2010) and Meneguz and Reeks (2010, 2011) report measurements of the moments at small St and St $= O(1)$ in simple periodic flows, kinematic simulations (with a distribution of energy and length scales typical of real turbulent flows) and in DNS of homogeneous isotropic turbulence. For small St the moments grow exponentially and smoothly with time, consistent with the behaviour predicted by Balkovsky *et al.* (2001). In contrast, the growth for St $= O(1)$ which, although the underlying trend is exponential, is dominated by spikes, indicating the momentary occurrence of singularities in the particle concentration in time (as has also been observed in simple 2-D linear flow fields of counter-rotating vortices; IJzermans *et al.*, 2009). They also observed a threshold value for St beyond which the average compressibility was negative rather than positive, meaning that the net continuum volume occupied by particles expands with time rather than contracts. However, this interesting feature belies other important features of the clustering process, since the exponential growth of the concentration moments persists despite the possible occurrence of a net negative compressibility indicating that there are always segregated regions where the particles are highly concentrated. The existence of this threshold from net compression to dilation was a feature common to all three flows investigated, suggesting that this transition may well be a property of particle flows in incompressible carrier flows in general, the transition depending upon the combination of local vorticity and straining encountered by a particle as it moves through the carrier flow. Measurements of the rate of occurrence of singularities (Meneguz and Reeks, 2010, 2011) show that it reaches a maximum at St $= 1$, with the distribution of times between singularities following a Poisson process.

For St $\ll$ 1, both Chun *et al.* (2005) and Zaichik and Alipchenkov (2003) predict that $g(r) \sim r^{-\tilde{\alpha}St^2}$, although the values of the constant $\tilde{\alpha}$ differ. This reflects a fundamental difference between the two approaches. The method of Chun *et al.* (2005) assumes that the form of $g(r)$ arises from a balance between turbulent diffusion and drift. The drift velocity they evaluate turns out to have the same form as that derived by Maxey (1987), who considered the difference in settling velocity in homogeneous isotropic turbulence due to preferential sweeping of the particles through turbulent structures in the direction of gravity (see also section 4.2.3 below). Although gravity had no influence in Chun *et al.* (2005), the Maxey formula also applies equally to the transport of particles in inhomogeneous turbulence: in this case the inhomogeneity is in the relative velocity of fluid elements as a function of their separation. In either case it involves the compressibility of the particle flow field along a particle trajectory. In contrast, the form derived by Zaichik and Alipchenkov (2003) is based on the droplet momentum equation (in the frame of reference moving with a colliding droplet) and in particular a force balance between the drag and the particle kinetic stresses. That is, given a uniform concentration of particles in an inhomogeneous flow, there would be a force acting on the particles due to gradients of the radial kinetic stresses. Because this force would be balanced by the drag force, which is proportional to the particle mean velocity, it would give rise to a drift velocity. The fact that both approaches give the same St dependence is coincidental. It turns out that the actual drift velocity is the sum of the two contributions (drift due to gradients in the radial kinetic stresses and local inhomogeneity in the instantaneous particle concentration).

Neither Chun *et al.* (2005) nor Zaichik and Alipchenkov (2003) take gravitational settling into account, which may decrease droplet clustering as it reduces the interaction time of a droplet with the turbulent eddies. This has been observed in DNS for sedimenting droplets (Vaillancourt *et al.*, 2002; Wang *et al.*, 2006a; Franklin *et al.*, 2007; Ayala *et al.*, 2008a). Falkovich *et al.* (2002) used a heuristic argument to include gravitational settling in their expression for $g(r)$. However, for bidisperse droplets, their formula is not closed, which makes it difficult to compare with other models.

A closed-form empirical formula for $g(r)$ that includes the effect of gravity has been proposed by Ayala *et al.* (2008b). In the monodisperse case, it may be expressed as (Chun *et al.*, 2005)

$$g(r) = C_0 \left(\frac{\eta}{r}\right)^{C_1}, \qquad (12)$$

which holds for $r \ll \eta$, the appropriate range for cloud droplets. This expression may hold for sedimenting droplets by assuming functional forms for C_0 and C_1 that depend on St, R_λ and Fr_f (Ayala *et al.*, 2008b). An empirical expression for C_1 was obtained by Ayala *et al.* (2008b) from their DNS data for $C_0 = 1$:

$$C_1 = \mathrm{Fr}_f^{f_1(R_\lambda)} f_2(\mathrm{St}), \qquad (13)$$

where $f_1(R_\lambda) = 0.1886 \exp(20.306/R_\lambda)$ and $f_2(\mathrm{St})$ is a fourth-order polynomial in St (with $f_2(0) = 0$). Any model of the RDF must have the correct form in several limiting cases: for weak-inertia particles, it follows from (12) and (13) that $g(r) \to 1$ as St $\to 0$. If $\mathrm{Fr}_f \ll 1$, i.e. the fluid acceleration is much less than the gravitational acceleration, or equivalently the limit of small ε, since $\mathrm{Fr}_f \sim \varepsilon^{3/4}$, then $C_1 \ll 1$ and $g(r) = 1$. In the limit $R_\lambda \to \infty$, C_1 depends only weakly on gravity. It is important to note that this model is a fit to DNS data for sedimenting cloud droplets where the droplet inertia and terminal velocity are related to one another (i.e. Sv and St increase together as a increases).

For non-sedimenting bidisperse droplets, clustering rapidly decreases as the difference in droplet size becomes larger (Zhou *et al.*, 2001; Woittiez *et al.*, 2009). The correlation between two droplets decreases with increasing difference in inertia as droplets with different inertia respond differently to changes in the flow. Thus the RDF of a bidisperse suspension is bounded above by the RDF of the monodisperse case. The DNS results of Woittiez *et al.* (2009)

show that the addition of gravity can cause droplets with slightly different sizes to cluster in different regions. Woittiez *et al.* (2009) also found that gravity facilitates the clustering of large droplets ($a \gtrsim 50$ μm), particularly monodisperse droplets–something which is not observed for non-sedimenting droplets. The precise reasons for this are not clear and the authors caution that the large-scale forcing and periodic boundary conditions employed in their DNS may introduce artefacts at large scales. We note here that when a nonlinear drag is assumed Ayala *et al.* (2008a) found that, for bidisperse droplets, there was no significant difference in droplet clustering compared with Stokes drag.

For a pair of droplets of two different sizes, any acceleration due to gravity or due to the turbulent fluid induces a relative velocity between the pair. This gives rise to a diffusive-like motion that tends to smooth out any inhomogeneities in the particle pair concentration and reduces the RDF. For bidisperse droplets, (12) can be extended to (Chun *et al.*, 2005; Ayala *et al.*, 2008b)

$$g_{12}(r) = C_0 \left(\frac{\eta^2 + r_D^2}{r^2 + r_D^2} \right)^{C_1/2},$$

where r_D is a parameter representing the diffusion-like process. If $r \ll r_D$, then $g_{12}(r)$ is independent of r, as expected when the acceleration-induced diffusion is important. Conversely, if $r \gg r_D$, then $g_{12}(r) = g(r)$ and the droplets in the pair both react similarly to the local acceleration. It is worth noting here that Lu *et al.* (2010) derived an analytical form of r_D (for St $\ll 1$) that is similar in form to that derived empirically by Ayala *et al.* (2008b). Moreover, Lu *et al.* (2010) extend the RDF of Chun *et al.* (2005) to include charged particles which compares well with experiments. The inclusion of electric charge allows the effect of gravity to be modified: as the difference in the settling velocities increases (by increasing the effective gravity), the RDF decays less rapidly with decreasing r.

As discussed in section 3.2, observations of droplet clustering in real clouds remain ambiguous, which has led some authors (e.g. Grabowski and Vaillancourt, 1999) to question its importance in real clouds. However, Shaw *et al.* (1999) argue that, although clustering of inertial particles tends to decrease rapidly with decreasing St $\lesssim 1$, there is some evidence (e.g. Reade and Collins, 2000) that the range of Stokes numbers for which clustering is significant increases with increasing R_λ. Shaw *et al.* (1999) argue that the vortex tubes that are associated with small-scale turbulence at high Reynolds numbers persist for longer than either τ_η or the large-eddy turnover time and so droplets with a much larger range of St are able to spin out of the vortex. The importance of intermittency in potentially increasing droplet clustering has also been raised by Falkovich *et al.* (2002). Based on theoretical arguments they found that clustering can increase collisions by a factor of ten. However, without a clear theoretical basis for the R_λ-dependence of clustering, which will remain valid in the large-R_λ limit, it is likely that these arguments will continue.

4.2.3. Preferential sweeping

Droplets falling under gravity in a turbulent fluid may fall at speeds which are significantly faster than their terminal velocity in a quiescent fluid (although under some conditions the speed of droplets may decrease relative to the terminal velocity; see section 4.2.6). Sedimenting (inertial) droplets can bias their trajectories towards regions of downward fluid motion around vortices: the crossing-trajectory effect (which occurs primarily because of sedimentation; Csanady, 1963) causes the particle to be preferentially swept to the downward side of the vortex and hence the mean effect of turbulence is a net force that accelerates the particle downwards. The increased settling occurs for Sv $\lesssim 1$ and a certain range of τ_p (Wang and Maxey, 1993; Dávila and Hunt, 2001).

The DNS results of Ayala *et al.* (2008a) show that the turbulent settling velocities of droplets with radii less than 40 μm are larger than the settling velocities in still air. They find that large droplets ($a \geq 40$ μm) have a mean velocity approximately equal to the terminal velocity and that droplets with $a = 20$ μm always exhibit the largest increase in settling velocity. The latter result can be explained by the analysis of Dávila and Hunt (2001) for inertial particles settling near a Rankine vortex. Dávila and Hunt (2001) introduced a particle Froude number, $\mathrm{Fr}_p = \mathrm{St}^3/\mathrm{Fr}_f^2 = \mathrm{St}\,\mathrm{Sv}^2 = \tau_p^3 g^2/\nu = \tau_p v_T^2/\nu$, which is independent of ε. They showed that for Sv < 1 and $\mathrm{Fr}_p \ll 1$ the turbulent settling velocity is always larger than the terminal velocity and that it increases with increasing Fr_p, reaching a maximum when $\mathrm{Fr}_p \sim 1$. For typical cloud conditions, $\mathrm{Fr}_p \approx 1$ for droplets with $a = 20$ μm. Thus the enhancement of the settling velocity reaches a maximum for $a = 20$ μm regardless of the value ε. In this case $\tau_p \approx \nu/v_T^2 = \nu_\eta \eta/v_T^2 = \tilde{\Gamma}_\eta/v_T^2 = \tau_\Gamma$, where $\tilde{\Gamma}_\eta$ is the circulation around an eddy of scale η and τ_Γ is the time-scale for the droplet to move around an eddy of order η. The time-scales τ_ν and τ_Γ have the same order of magnitude when Sv ~ 1.

4.2.4. Droplet–droplet interactions

In reality, interactions between droplets (hydrodynamic or aerodynamic interactions) play an important role in cloud physics particularly for droplets with radii less than 60 μm which have a short inertial response time and small settling rate (Wang *et al.*, 2006b). In the case of a quiescent fluid, the collision kernel for two droplets falling under gravity alone (6), may be modified to give

$$\Gamma_{12} = \pi r_c^2 |v_{T2} - v_{T1}| E_{12}(a_2/a_1, a_2),$$

where E_{12} is the collision efficiency (ignoring changes in the density and viscosity of air with height). The qualitative shape of $E_{12}(a_2/a_1, a_1)$ may be anticipated from the following considerations (Pruppacher and Klett, 1997, p. 571). Viscosity tends to ensure that the smaller of the two droplets (with radius a_2) moves around the larger droplet (with radius a_1) and hence is deflected from the collision trajectory. Thus, in general, one would expect that $E_{12} < 1$. With increasing inertia, this deflection becomes less likely and hence E_{12} should be a monotonically increasing function of a_1. Similarly for increasing a_2/a_1, at least when $a_2/a_1 \ll 1$. As $a_2/a_1 \rightarrow 1$, the situation becomes more complex as the relative velocity decreases and allows more time for viscous forces to act and hence prevent a collision. On the other hand, the trailing droplet may fall into the wake of the leading droplet, *wake capture*, which may increase E_{12} to values greater than one.

Compared with the study of geometric collision rates, there have been relatively few studies of the effect of

turbulence on droplet–droplet interactions. The geometric collision kernel (9) can be modified to account for droplet–droplet interactions by defining a turbulent collision efficiency (Wang *et al.*, 2005b, 2006b; Pinsky *et al.*, 2007):

$$E_{12} = \frac{\Gamma_{12}(\text{HI})}{\Gamma_{12}(\text{No HI})}, \qquad (14)$$

where 'HI' and 'No HI' respectively indicate that Γ_{12} has been computed with or without droplet–droplet interactions (keeping all other pertinent quantities fixed). In terms of the radial relative velocity and the RDF (14) becomes

$$E_{12} = \frac{\overline{|w_{12}(\text{HI})|}g_{12}(\text{HI})}{\overline{|w_{12}(\text{No HI})|}g_{12}(\text{No HI})},$$

with the dependence on r_c now implied rather than explicit.

Pinsky *et al.* (1999b) proposed a mathematical formulation to study the effect of far-field turbulent fluctuations on droplet–droplet interactions. Working in a frame of reference moving with the local air flow, they proposed the addition of a far-field inertia-induced turbulence contribution, $\tau_p dU/dt$, to the droplet–air relative motion, where U is the undisturbed local air flow velocity. Their main conclusion is that the collision efficiency in a turbulent flow is a random number with a mean value that is typically larger than the gravitational collision efficiency, due to turbulence-enhanced droplet–droplet relative velocity and the associated variation of the droplet–droplet angle of approach (see also Wang *et al.*, 2006c). Their formulation relies on a number of assumptions, including that St is very small, the inertia-induced relative motion has a time-scale much greater than the time-scale associated with droplet–droplet interaction and the two interacting droplets remain in the same dissipative eddy during the whole time interval of their interaction. These assumptions are not always valid for large ε or large droplet size. Furthermore, their turbulent flow was kinematically constructed as a two-dimensional frozen pseudo-turbulent flow generated by a large number of random Fourier modes designed to yield the desired inertial-to-dissipation range energy spectrum. This flow model does not adequately describe the fine structure of a turbulent flow and leads to an overestimation of the magnitudes of the Lagrangian accelerations as noted in Pinsky and Khain (2004). For these reasons, Pinksy *et al.* (1999b) stated that their results should be viewed as 'qualitative to a certain degree'.

Pinsky *et al.* (2001) recognized that the droplet terminal velocity can increase with height (decreasing ambient air pressure and density) and this will increase the relative motion between a pair of droplets. They showed that a small change (5% to 20%) in the relative velocity due to the decreased ambient pressure could lead to a significant increase (up to a factor of two) in collision efficiency. They introduced an approximate representation of disturbance flow at finite-droplet Reynolds numbers and calculated the collision efficiency between droplets of radius up to 300 µm at several ambient pressures (100, 750 and 500 mb).

Using the same approximate formulation of Pinksy *et al.* (1999b), Pinsky and Khain (2004) studied the effects of fluid accelerations at high-flow Reynolds numbers. They showed that the collision efficiency for collector droplets exceeding 10 µm can be increased by 25–40% for $\varepsilon = 200$ cm^2 s^{-3} and by a factor of 2.5–5 at $\varepsilon = 1000$ cm^2 s^{-3}. They also showed that the effect of intermittency on collision efficiency is insignificant. However, it appears that they misinterpreted the fluid acceleration seen by a droplet as the Lagrangian fluid acceleration. This misinterpretation may be problematic for high R_λ flow, even in the limit of small St number.

Wang *et al.* (2005b) proposed a hybrid DNS approach to modelling hydrodynamic interactions based on the superposition method. This method (Pruppacher and Klett, 1997, p. 571) assumes that each sphere moves in a flow field generated by the other sphere falling in isolation. However, it becomes inaccurate when the separation distance between the two droplets is comparable with the collision radius. Wang *et al.* (2005a) formulated a revised superposition method which avoids this limitation by imposing proper boundary conditions on the surface of the droplets. The hybrid DNS results of Wang *et al.* (2005b), with the revised superposition method, show that air turbulence increases both the geometric collision rate and the collision efficiency, particularly as $a_2/a_1 \rightarrow 1$. They found that the results depend sensitively on the size of the larger droplet. Relative to a quiescent fluid, for $a_1 = 30$ µm, the geometric collision rate is more enhanced than the collision efficiency, whereas for $a_1 = 20$ µm the situation is reversed. They observed that hydrodynamic interactions are less effective at reducing the average droplet relative velocity in a turbulent flow compared with sedimenting droplets in a quiescent flow. For this reason, turbulence enhances the collision efficiency as well as the geometric collision rate. Hydrodynamic interactions also increase the pair density in the vicinity of the collision, giving a higher RDF at contact compared with geometric collisions. Wang *et al.* (2006b) also noted that the collision efficiency among equally sized droplets depends on the presence of differently sized droplets in the suspension–a cumulative effect of all the droplet interactions in the flow. This means that theoretical treatments of hydrodynamic interactions that are based on two isolated droplets may not be applicable to a suspension of many droplets, even in the absence of turbulence.

Another revised formulation of the superposition method has been proposed by Pinsky *et al.* (2007). They decomposed the droplet velocity (relative to the fluid) into an undisturbed part (without the impact of the other droplet) and a disturbed part, representing the velocity induced by the other droplet. They obtained two equations of motion for each of the two velocities and simplified the equation for the undisturbed velocity by assuming that it is equal to its quasi-stationary value. They justified this assumption by assuming that the collision between the two droplets takes place in an elemental volume in which the droplet velocity relaxes to its quasi-stationary value on a time-scale shorter than that on which the fluid velocity is changing. Pinsky *et al.* (2007) examined the pdf of the instantaneous collision efficiency for a droplet pair with radii 10 and 15 µm for three different cloud types, stratiform ($R_\lambda = 5000$, $\varepsilon = 10$ cm^2 s^{-3}), cumulus ($R_\lambda = 20\,000$, $\varepsilon = 200$ cm^2 s^{-3}) and cumulonimbus ($R_\lambda = 20\,000$, $\varepsilon = 1000$ cm^2 s^{-3}) (see Figure 6 in Pinsky *et al.*, 2007). They found that the tails of the pdf become increasingly elongated as ε increases, particularly if the statistics of the acceleration and velocity gradients were assumed to be non-Gaussian. For both cumulus and cumulonimbus clouds, they found that the pdf becomes positively skewed, indicating that turbulence may increase the local collision efficiency

considerably. For cumulonimbus clouds they showed that the mean collision efficiency relative to purely gravity-induced collision efficiency can be greater than a factor of three (see Figure 10 in Pinsky *et al.*, 2007).

4.2.5. Random uncorrelated motion: its relationship to the formation of caustics and singularities

Sundaram and Collins (1997) recognized that both clustering and velocity decorrelation between particle pairs have an important influence on inter-particle collisions: clustering enhances the neighbouring concentration of particles about any given particle and the velocity decorrelation between particles causes two nearby particles to collide (other than through interception). Since the interplay between these two effects determines the collision rate in a turbulent flow, it is essential to quantify as accurately as possible not only the clustering but also the mechanism that lies behind the increase in the relative velocity between adjacent particles. Stokes disturbance flow is known to have extended long-range effects: the finite response time of inertial particles in turbulent flows means that droplets can retain a memory of a fluid eddy with which it has previously come into contact. This means that the particle velocity contains an element that is non-local and uncorrelated with the local fluid. Based on their studies of particle motion in DNS turbulence, Février *et al.* (2005) and Masi *et al.* (2010) partitioned the particle motion into a spatially random uncorrelated motion (RUM) and a mesoscopic motion derived from a smoothly varying particle velocity field which is responsible for the spatially correlated part of the particle motion. By measuring the spatial velocity correlation between pairs of particles, they were able to calculate the contribution the RUM and the mesoscopic velocity fields make to the particle's turbulent kinetic energy and how this varied with St. This feature is attributed to the ability of the trajectories of particles with inertia to cross one another with different and uncorrelated velocities as these particles retain the memory of their interaction with very distant and statistically independent eddies in the flow field. It is RUM that allows droplets to collide. Falkovich *et al.* (2002) recognized this feature of particle motion, showing that in the limit St $\ll$ 1 droplets that overlap exhibit different velocities. They described this as particles being spun out of regions of vorticity and collecting together with different velocities at the moment of contact (as a consequence of their different histories of motion). They referred to this process as the *sling-shot effect*. We note also the analogy with the concept of free flight to the wall (Brooke *et al.*, 1994) used to explain the deposition of particles in turbulent boundary layers.

The occurrence of singularities and RUM is contrary to the commonplace picture of clustering as a local process intimately related to the local straining and vorticity of the carrier flow. What these features have highlighted is the opposite and in particular a consequence of a particle's memory of many encounters with straining and vorticity regions in the flow. RUM is entirely non-local and so is the occurrence of singularities. Important in this regard is the analysis of Wilkinson and Mehlig (2005), who considered particle motion in a mixture of potential and solenoidal flows that lead to the existence of a filamental network of caustics (where the particle velocity field becomes multi-valued) with a very high accumulated concentration of particles at the edges and within which particle trajectories cross. While their analysis was only strictly applicable to flows with a Kubo number (Ku, defined as the ratio of the velocity decorrelation time-scale to the sweeping time-scale) of zero, it suggested a strong link between the existence of singularities and the occurrence of RUM, i.e. that they coexist in the same region. Recent investigations using the fully Lagrangian and similar methods would appear to confirm this relationship (e.g. Ducasse and Pumir, 2009). Singularities in the particle velocity field can lead to greatly enhanced collision rates (because droplets at the same position can have different velocities). For large Reynolds numbers this effect could be as important as the effects of intermittency in fluid accelerations, which can also cause extreme peak values in droplet collision rate fluctuations (e.g. Shaw and Oncley, 2001).

Wilkinson *et al.* (2006) argued that the process of droplet coalescence and growth cannot be explained in terms of particle clustering, firstly because this mostly occurs when St $\sim$ 1 (whereas typically St $\ll$ 1 for cloud droplets), and secondly because the volume loading of droplets in a cloud is very low and so it would be hard to find particles at separation distances of order η. Instead they proposed that the collision kernel be composed of two parts:

$$\Gamma = \Gamma_a + \exp(-A/St)\,\Gamma_g,$$

where Γ_a is a collision kernel appropriate for tracer particles, i.e. (7), and the second term on the right-hand side is an additional kernel arising from the activation of caustics. Here, Γ_g is the collision kernel based on the kinetic theory of gases for totally random trajectories (Abrahamson, 1975) and A depends on Ku and has a value of 0.7 for Ku = 1, which is appropriate for real turbulence. The term $\exp(-A/St)$ describes the fraction of space for which the velocity field has become multi-valued (due to the formation of caustics). This formulation of the collision kernel has much in common with the decomposition of the particle velocity field into its mesoscopic and RUM components. Their kernel leads to an increase in the collision rate through the crossing-trajectory effect which occurs when the dimensionless turbulence intensity (which is proportional to St) exceeds the action for forming caustics. Note, however, that it is Γ_a that is the dominant term when St $\ll$ 1, which is the more appropriate limit for most cloud droplets.

4.2.6. Laboratory experiments

There have been a number of advances in experimental studies of inertial particles in turbulent flows in recent years (e.g. Warhaft, 2009). In this section we provide a brief overview of recent results.

There is very strong evidence for inertial particle clustering from laboratory experiments in both 'box' turbulence (homogeneous turbulence without a mean flow) and in wind tunnel turbulence. In box turbulence, Wood *et al.* (2005) show, from the 2-D RDF for $0.57 \le$ St ≤ 8.1, that particle clustering peaks for St $\sim$ 1 and for scales less than approximately 10η. The numerical values of the 2-D RDFs were not in quantitative agreement with earlier DNS but this was attributed to the reduction in dimension of the measurement (Holtzer and Collins, 2002). Yang and Shy (2005) also show that, for $0.3 \le$ St ≤ 1.9, clustering is greatest for St $\sim$ 1. Salazar *et al.* (2008) and de

Jong *et al.* (2010) study (experimentally) the full 3-D RDF for $0.21 \leq St \leq 0.6$ and the former also provide excellent confirmation of their clustering measurements at the small scales using DNS. All of these box turbulence measurements were made for R_λ of the order of a few hundred.

Saw *et al.* (2008) determined the 1-D RDF in a wind tunnel with water sprays for an St range from 0.3 to 1.5 at $R_\lambda \approx 500$. They too find that the clustering is strongest for scales less than 10η and for $St \sim 1$, although in these and in the other experiments reported here there is significant clustering at lower St. The results of Saw *et al.* (2008) show scale separation of inertial-range clustering due to mixing and dissipation-range clustering due to inertia. The behaviour of bidisperse and polydisperse RDFs were found to be in good agreement with DNS (Saw, pers. comm., 2011). By analysing Voronoi diagrams of wind tunnel data, Monchaux *et al.* (2010) also find that clustering peaks at $St \sim 1$. Both DNS and experiment show that the RDF approaches a plateau at small separations and the exponent of the bidisperse RDF approaches that of the equivalent monodisperse RDF for the particle with the smaller Stokes number.

There have also been a number of experiments on the particle-settling velocity in turbulence. Aliseda *et al.* (2002) and Yang and Shy (2005) show enhanced particle-settling velocities which are consistent with the numerical work of Wang and Maxey (1993). Gerashchenko *et al.* (2011) show the strong effects of gravity on the selective transport of particle sizes by changing the orientation of the apparatus in the gravitational field. Good *et al.* (2011) show that the particle-settling velocity can either be enhanced or diminished (in comparison with the terminal velocity in a quiescent fluid) depending on the value of Sv. When the turbulence is weak relative to the terminal velocity the settling speed is diminished, while if it is strong it is enhanced. These results confirm earlier findings of Nielsen (1993).

Lagrangian measurements of inertial particles using particle tracking techniques (Ayyalasomayajula *et al.*, 2006) show that as St is increased the tails of the particle acceleration pdf become narrower compared with those of fluid particles. These results are supported by the DNS of Bec *et al.* (2006). Nevertheless, the tails are still strongly stretched compared with those of a Gaussian distribution and become increasingly so with increasing R_λ. Ayyalasomayajula *et al.* (2008) show that there is a clear connection between the particle acceleration pdf and clustering: the inertial particles selectively sample the flow field, oversampling regions with high strain and undersampling regions with high vorticity. At low St (pertaining particularly to cloud droplets) this biased 'sampling' of the flow is responsible for the reduction in the particle acceleration variance and, to first order, explains the attenuation of the tails of the acceleration pdf.

4.2.7. Impact of turbulent collision–coalescence on droplet growth and warm rain initiation

Several attempts have been made to address specifically the impact of selected aspects of air turbulence on the time evolution of the droplet size spectrum. Typically, these studies begin with an empirical formulation or tabulated data of the turbulent collision kernel that exceeds the gravitational collision kernel. Pinsky and Khain (2002)

demonstrated that collision kernels taking into account the effect of air turbulence on the relative motion of droplets can lead to the acceleration of large droplets and raindrop formation. Falkovich *et al.* (2002) proposed a semi-analytical kernel that includes the effects of clustering of droplets and local fluid acceleration due to cloud turbulence and showed that cloud turbulence could substantially accelerate the formation of large droplets. Ghosh and Jonas (2001) applied the ideas of Dávila and Hunt (2001) on preferential sweeping (see section 4.2.3) to an approximate equation for droplet growth and found that the results compared favourably with observations of stratocumulus. Ghosh *et al.* (2005) argued that the preferential sweeping of droplets in clouds could make droplets grow rapidly from 20 μm to 80 μm and that this occurs irrespective of the level of cloud turbulence (see also section 4.2.3). These studies, however, are based on phenomenological formulations of the turbulent collision kernel.

Turbulent collision kernels derived from DNS data have also been used to study droplet growth. Franklin (2008) studied the mass conversion rate of cloud droplets to raindrops by solving the stochastic coalescence equation with the use of turbulent collision kernels. She observed that the conversion rate increases with increasing flow dissipation rate. Hsieh *et al.* (2009) calculated the conversion rate using the turbulent collision kernel of Ayala *et al.* (2008b) and found that turbulence effects can increase the conversion rate by a factor of 1.24 to 1.82 for two specific initial cloud droplet size distributions, relative to purely gravitational collection. Figure 2 shows the typical effect of turbulence on the collision kernel relative to a purely gravitational collision kernel both in its totality and broken down into its constituent parts, i.e. the individual effects of the droplet relative velocity, droplet clustering and collision efficiency. Figure 2 shows a noticeable enhancement for $\varepsilon = 200$ cm^2 s^{-3} and droplets less than 100 μm, although the overall enhancement is moderate, with a value ranging from 1.3 to 2.6 for most regions (Grabowski and Wang, 2009). This enhancement factor increases with increasing ε with, for example, the typical enhancement factor varying between one and five for $\varepsilon = 400$ cm^2 s^{-3}. Figure 2 also shows that the dominant contribution to the enhancement factor comes from droplet clustering and the collision efficiency. However, the droplet relative velocity plays an important role in facilitating collisions between droplets of comparable size.

The levels of enhancement found by Grabowski and Wang (2009) and replicated in Figure 2(a) can be compared with the tabulated results in Pinsky *et al.* (2008a), who compiled collision kernel enhancement factors by turbulence for droplets in the size range from 1 to 21 μm and ε in the range 10–1000 cm^2 s^{-3} (based on the formulation developed in Pinsky *et al.*, 2007). For $\varepsilon = 200$ cm^2 s^{-3}, Pinsky *et al.* (2008a) found that the enhancement factors can vary from approximately 1.5 to approximately 8, with an average value around 2–3. In Grabowski and Wang (2009) the enhancement factors for droplets with $a = 21$ μm or less are in the range 1.2–1.6 at $\varepsilon = 100$ cm^2 s^{-3} and 1.5–4.5 at $\varepsilon = 400$ cm^2 s^{-3}. Thus the values of Pinsky *et al.* (2008a) are comparable with those in Figure 2 with a somewhat larger range of variation. This shows that different approaches appear to lead to similar levels of enhancement factors by air turbulence.
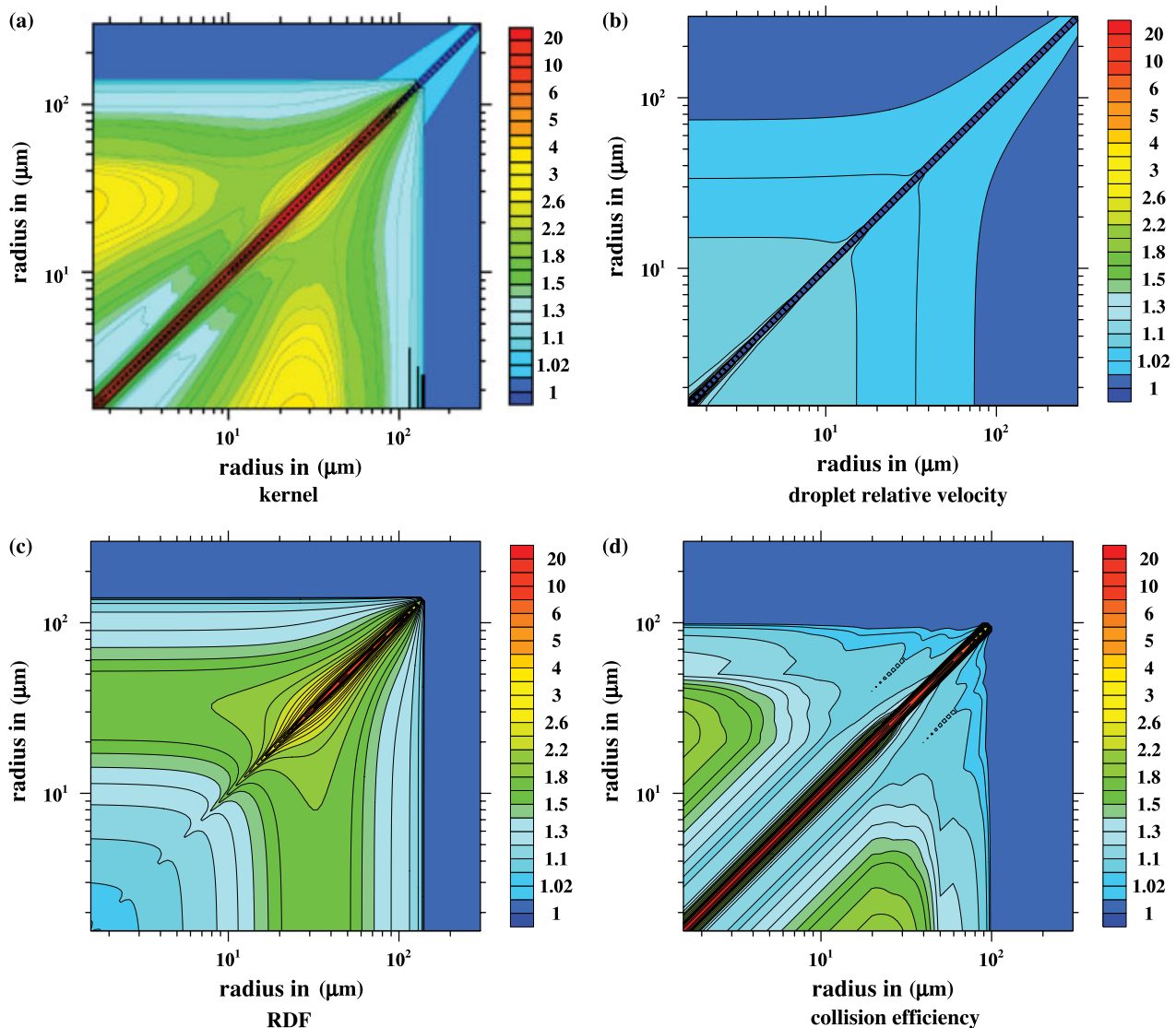
Figure 2. (a) The ratio of a typical turbulent collision kernel to a purely gravitational collision kernel (Wang and Grabowski, 2009) for $\varepsilon = 200$ cm^2 s^{-3}. The ratio on the 45° degree line is undefined owing to the zero value of the gravitational kernel. The ratio is essentially one when droplets are greater than 100 µm. The constituent parts of the turbulent collision kernel are shown in (b) the droplet relative velocity, (c) the RDF and (d) the collision efficiency.

The values shown in Figure 2 should be taken as preliminary results owing to the limitations of DNS, as noted in Pinsky *et al.* (2007), Ayala *et al.* (2008a) and Wang *et al.* (2008). The most significant limitation is that not all scales of turbulence affecting droplet–droplet interactions are included in DNS, making the enhancement factors shown in Figure 2 most likely a lower bound of what might occur in real clouds. A related issue is the effect of flow intermittency at high flow Reynolds numbers, which requires further investigation. The study of Pinsky and Khain (2004) suggests that the effect of flow intermittency is not significant owing to the very low probability of large local fluctuations. However, as discussed above, this neglects the possibility of a 'lucky droplet' that benefits from such a rare event. A nonlinear drag law is also needed to describe the motion of large droplets, as done in Ayala *et al.* (2008a).

By solving the stochastic coalescence equation using an accurate bin integral method with the turbulent collision kernel of Ayala *et al.* (2008b), Xue *et al.* (2008) showed that, under conditions typical of cumulus clouds, air turbulence can shorten the time for the formation of drizzle drops by 20–40% relative to gravitational collection alone. When the

effect of turbulence on collision efficiency is also considered, Wang and Grabowski (2009) concluded that the warm rain initiation time could be reduced up to a factor of two. Using the same turbulent collision kernel and a rising adiabatic parcel model that combines droplet activation, diffusional growth and turbulent collision–coalescence, Grabowski and Wang (2009) showed that air turbulence could reduce the warm rain initiation time by 25–40%. Seifert *et al.* (2010) incorporated the turbulent collision kernel of Ayala *et al.* (2008b) in LES of small cumulus clouds and found that this led to an increase in the production of rain. They also found that the effect was most pronounced near the cloud top, where dissipation rates tend to be highest. This region plays a decisive role in the initial formation of rain and shows that dissipation rates correlate well with the liquid water content.

5. Effect of entrainment on droplet size distribution

The very narrow droplet spectra that are a consequence of (2) (and serve as a reference against which all broader droplet spectra are compared) would only exist in reality if all

the droplets experienced the same supersaturation or, more precisely, the same integral of the supersaturation along their trajectories (as follows from (2)). The quasi-adiabatic core of cumulus clouds most closely approximates such an idealized situation in which the droplets are activated at cloud base and grow in a closed convective cell. In reality, convective cells are not adiabatically closed and turbulence continuously mixes droplets that have followed different trajectories and so have different supersaturation histories, resulting in broader spectra than in a purely adiabatic cell. Thus very narrow (adiabatic) spectra are likely to be the exception rather than the rule; indeed, airborne cloud traverses show that narrow spectra are only observed when the liquid water content is high and close to its adiabatic value. Moreover, when enough dry air is entrained and mixed with a cloudy parcel, some droplets can evaporate completely. If this parcel then experiences a strong updraught, the remaining droplets might not be able to fully deplete the available water vapour and new CCN can be activated, thus producing small droplets. Indeed, bimodal spectra have long been observed in regions of diluted liquid water content (e.g. Warner, 1969a).

Brenguier and Grabowski (1993) developed a model that is useful for examining the impact of entrainment on droplet spectra in LES of realistic clouds. When the effects of small-scale turbulence are neglected, all droplets in a given cloud volume are exposed to the same supersaturation, which means that their surface growth rates are equal (a consequence of (2)). In other words, the magnitude of the droplet surface distribution, $f(a^2)da^2$, is changed by condensation or evaporation but its shape is kept constant. Assuming a given initial droplet spectrum after CCN activation, $f_0(a^2)da^2$, the droplet spectrum in any adiabatic cell can thus be expressed as $f(a^2)da^2 = f_0(a^2 - b^2)da^2$, where b^2 is proportional to the integral of supersaturation along the droplet trajectory. Mixing between grid boxes in LES is accounted for by the pdf of b^2, which is calculated on an Eulerian grid. The b^2 distribution in a given grid box describes the proportion of droplets of different sizes which have experienced the same amount of diffusional growth. The results of a 2-D simulation of a cumulus cloud (see Figures 6, 7 and 8 in Brenguier and Grabowski, 1993) show a large variability of b^2 distributions, with narrow ones in the core of the updraught, while bimodal distributions with a peak at low values of b^2 reflect the impact of new CCN activation on the droplet spectra. Note also that, while the initial effects of entrainment are noticeable at the cloud edge, they can also affect the core of the cloud when enveloped by large eddies. Such Eulerian simulations illustrate the strong constraints large-scale thermodynamics (at the LES grid scale) impose on simulations of the small scales alone.

Problems with the comprehensive representation of physical and thermodynamic processes in Eulerian LES and cloud-resolving models (associated with both model complexity and numerical aspects such as numerical diffusion) have prompted an interest in Lagrangian methods where some of these difficulties can be overcome. The idea is to combine an Eulerian fluid-flow model with an ensemble of Lagrangian fluid trajectories. Such methods have been quite successful in explaining some aspects of the impact of turbulence on cloud microphysics (see, for example, the discussion in Stevens *et al.*, 1996; Feingold *et al.*, 1998; Lasher-Trapp *et al.*, 2005; Pinsky *et al.*, 2008b; Magaritz *et al.*, 2009). However, the main problem

with such approaches is that, in a turbulent environment, a fluid parcel loses its identity relatively quickly. If the fluid parcel is assumed to have spatial extent l, then such a parcel can keep its identity up to approximately time t_l given by $t_l \sim (l^2/\varepsilon)^{1/3}$. Taking $l \sim 10$ m and $\varepsilon \sim 10$ cm^2 s^3–reasonable choices for atmospheric boundary layer flows–one gets $t_l \sim 1$ min. It follows that results from such models need to be treated with much caution unless interactions among the parcels are explicitly included, which is typically not the case. Recently, a different Lagrangian approach was developed, with the focus not on air parcels but on particles carried by the flow such as cloud droplets. In such an approach, the Eulerian fluid flow model is coupled to the Lagrangian representation of the thermodynamics (see, for example, Andrejczuk *et al.*, 2008, 2010; Shima *et al.*, 2009). This approach is in the spirit of the pseudo-LES simulations presented in Lanotte *et al.* (2009) and discussed in section 4.1.3.

5.1. Homogeneous and inhomogeneous mixing

Airborne observations (e.g. Warner, 1955, 1969a, 1969b; Blyth *et al.*, 1988; Gerber *et al.*, 2005, 2008; Burnet and Brenguier, 2007; Haman *et al.*, 2007) tend to show that stratocumulus is only slightly diluted by entrainment, whereas cumulus is much more strongly diluted. In cumulus clouds the droplet number concentration is less reduced by entrainment than the liquid water content because the majority of droplets exhibit some evaporation. In stratocumulus, on the other hand, entrainment dilutes the droplet number concentration and the liquid water content by a similar amount, while the size of the droplets is relatively unaffected compared with cumulus clouds (e.g. Burnet and Brenguier, 2007).

Latham and Reed (1977), Baker and Latham (1979) and Baker *et al.* (1980) characterized mixing in terms of the relative time-scales of droplet evaporation and turbulent homogenization of a given control volume. If the length scale of the control volume lies within the inertial subrange of turbulence, then the ratio of these two time scales is the Damköhler number introduced in section 4.1. When Da $\gg$ 1, thermodynamic changes to the droplets occur on faster time-scales than any turbulent mixing and the mixing is said to be inhomogeneous. In this case, evaporation does not occur uniformly throughout the control volume and a fraction of the droplets in part of the control volume may evaporate completely, whereas other droplets are unaffected by thermodynamic changes. In the inhomogeneous limit, sometimes referred to as extreme inhomogeneous mixing, the number of droplets decreases but their size remains fixed. When Da $\ll$ 1, the turbulent mixing of droplets takes place on a faster time-scale than thermodynamic changes to the droplets and the mixing is said to be homogeneous. In this case the rate of droplet evaporation is the same for all droplets and so the number of droplets remains constant (but not their density, n, which decreases with dilution) but their mean size decreases. The choice of control volume clearly determines the turbulent mixing time-scale and hence the degree to which mixing is homogeneous or inhomogeneous, a point we return to below. A further factor concerns the point in the evolution of the cloud at which the measurements are taken: intuitively one may expect mixing to become more inhomogeneous as the cloud becomes less vigorous.
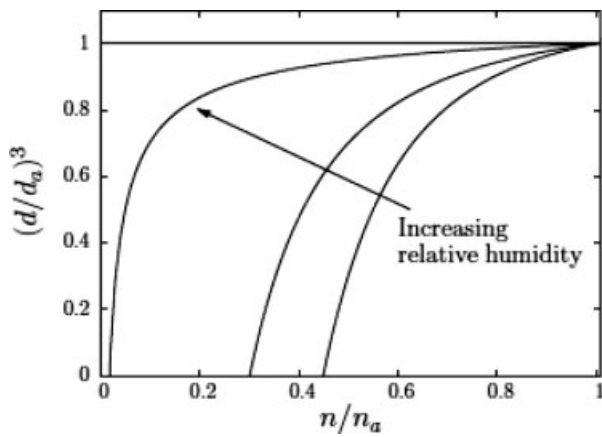
Figure 3. Schematic example of a mixing diagram. The horizontal dashed line indicates inhomogeneous mixing and the solid lines indicate homogeneous mixing for different relative humidities (saturation deficits) of the entrained air. The suffix a refers to adiabatic values and d is the droplet diameter.

As the liquid water content is proportional to $\overline{na^3}$, the microphysical properties of mixing can be examined on a mixing diagram as shown schematically in Figure 3, in which the abscissa is n and the ordinate is proportional to the mean droplet volume, both normalized by their respective adiabatic values (Burnet and Brenguier, 2007). The inhomogeneous limit then appears as a horizontal line on this diagram, while homogeneous mixing is represented by curved lines for different values of the relative humidity, or saturation deficit (negative s), of the entrained air (note that the final mixture returns to equilibrium i.e. $s = 0$). Different points along these lines represent different fractions of entrained and cloudy air (lines of constant mass fraction of cloudy air would appear as vertical lines on the mixing diagram in Figure 3; see also Figures 1 and 2 of Burnet and Brenguier, 2007). When the entrained air is close to saturation, i.e. for relative humidities greater than 90%, there is almost no difference between homogeneous and inhomogeneous mixing (except when n/n_a is small).

Lehmann *et al.* (2009) argue that the classification of mixing in terms of a single Damköhler number may be ambiguous since there is no *a priori* reason to fix a mixing length scale and hence τ_r. As turbulence consists of a spectrum of eddy sizes, in any given cloud the mixing could be inhomogeneous at some scales and homogeneous at other scales. Since $\tau_s \lesssim 10$ s, mixing at scales greater than several metres will be inhomogeneous but not necessarily at centimetre scales. A length scale, $l_c = \varepsilon^{1/2}\tau_s^{3/2}$, can be defined (Baker *et al.*, 1980; Lehmann *et al.*, 2009) at which there is a transition from inhomogeneous to homogeneous mixing (i.e. Da = 1). Observations of cumulus by Lehmann *et al.* (2009) show that there are regions of high ε where the transition length scale is greater than 10 cm. Entrainment leads to a decrease in buoyancy of the cloud, which in turn decreases ε. Hence the mixing time-scale increases and l_c decreases, implying that mixing is more likely to be inhomogeneous. However, there is some evidence (e.g. Siebert *et al.*, 2006a, 2006b) that ε is higher around the cloud edges than in the cloud core, perhaps as a result of the initial entrainment, which would suggest that l_c is larger near the cloud edge (leading to a greater prevalence of homogeneous mixing). In general, though, one would expect that over a sufficiently long time

period ε would decrease as a result of mixing. The type of mixing near the cloud edge also depends on the amount of dilution of the cloud due to entrainment of dry air, with the mixing in cumulus being homogeneous when the dilution is low but becoming more inhomogeneous as the dilution increases (Burnet and Brenguier, 2007). Comparisons of stratocumulus and cumulus by Burnet and Brenguier (2007) (in which the turbulent homogenization time-scale, τ_r, and the evaporation time-scale, τ_e are calculated for a length scale of 10 m) show that mixing in stratocumulus appears more inhomogeneous than in cumulus: values of ε tend to be lower in stratocumulus compared with cumulus, hence the value of l_c is, on average, smaller in stratocumulus than in cumulus, which explains why inhomogeneous mixing is more likely in stratocumulus compared with cumulus.

Lasher-Trapp *et al.* (2005) considered the effect of entrainment on the droplet size distribution in LES of a cumulus cloud. They used a Lagrangian stochastic model (which introduces subgrid variability) to calculate the trajectories of fluid particles along which they calculated the supersaturation, which in turn was used to calculate the growth of cloud droplets. Droplet size distributions at a given location in the cloud were calculated from an ensemble of trajectories reaching that point. Their model allowed for explicit variation of the degree to which mixing was assumed to be homogeneous or inhomogeneous (see equations (7) and (9) in Lasher-Trapp *et al.* (2005) and the attendant discussion for details). They found that for purely homogeneous mixing (see Figure 6 of Lasher-Trapp *et al.*, 2005) entrainment led to a broadening of the droplet size distribution near the cloud top, with a peak occurring at a value of a several microns larger than for a control simulation with adiabatic ascent alone (no entrainment). As the degree to which the mixing became more inhomogeneous, so the number of smaller droplets increased with a bimodal structure emerging for 20% inhomogeneous mixing (see Figure 7 of Lasher-Trapp *et al.*, 2005). For 100% inhomogeneous mixing the dominant mode occurs at a value of a several microns smaller than both the homogeneous and adiabatic cases. Lasher-Trapp *et al.* (2005) attribute this to the dominance of entrained CCN rather than droplets formed at cloud base. The importance of entrainment in broadening the droplet size distribution can be appreciated by comparing the droplet size distribution at a central point in the cloud early in its evolution, which is close to its adiabatic form, with a droplet size distribution near the cloud top (which exhibits significant broadening). However, Lasher-Trapp *et al.* (2005) do not consider particle inertia or sedimentation in their simulations. Moreover, their method does not account for mixing between different Lagrangian particle trajectories except at the end point (each particle is treated independently of the other particles) and so a droplet may experience a more favourable environment for growth than would otherwise be the case if mixing were allowed. Hence, as Lasher-Trapp *et al.* (2005) acknowledge, their method can produce an overestimation of droplet spectra broadening.

Homogeneous and inhomogeneous mixing has also been studied in DNS (e.g. Andrejcuk *et al.*, 2004, 2006, 2009; Malinowski *et al.*, 2008) and using pdf methods (Jeffery and Reisner, 2006; Jeffery, 2007). From DNS of cloud–clear air interfacial mixing with a range of initial kinetic energy levels, mixing fractions of cloudy and clear air, relative

humidities and droplet sizes, Andrejczuk *et al.* (2009) found a strong correlation between the instantaneous value of Da and the instantaneous rate of change of the droplet number concentration with droplet volume. Andrejczuk *et al.* (2009) observe a power law scaling when they plot dn/da^3, the gradient on the mixing diagram in Figure 3, against Da (see Figure 2 in Andrejczuk *et al.*, 2009). They find that the range of Da for which the power law scaling holds best is similar to the range for which the model of cloud front evaporation by Jeffrey and Reisner (2006) predicts the maximum correlation (magnitude) between subsaturation and droplet concentration at the cloud front. For Da ≈ 5, Jeffery (2007) predicts that mixing changes from inhomogeneous to homogeneous which is similar in magnitude to the transition value of Da for the DNS results of Andrejczuk *et al.* (2009).

5.2. Mechanisms for entrainment in clouds

Bulk (average) modelling of the effects of condensation and evaporation is commonplace in cloud-resolving models where the typical resolution may be tens or hundreds of metres. In this approach, the change in the amount of water vapour due to condensation or evaporation is equal to the amount required to maintain exact saturation over the model grid box. However, this approach neglects the possibility that a grid box whose mean water vapour mixing ratio is saturated or supersaturated may have filaments of strongly subsaturated air at subgrid scales as a result of entrainment.

The entrainment process proceeds first by the engulfment of dry air by the turbulent cloud which, through the action of turbulence, gradually forms filaments of dry and cloudy air and finally homogenizes the mixture when the filaments approach the Kolmogorov scale. As discussed in the previous subsection, homogenization does not occur instantaneously and the time-scale on which it occurs is important because evaporative cooling may lead to buoyancy reversal. Since observations suggest that mixing in cumulus clouds is more homogeneous than in stratocumulus, the mixing (filamentation) process takes place more rapidly in cumulus than in stratocumulus. The modelling of the entrainment process has been considered in the context of linear-eddy models by Krueger (1993), Krueger *et al.* (1997) and Su *et al.* (1998). These studies highlight the importance of small-scale mixing: a broader droplet spectrum and larger droplet formation occurred for mixing on a finite time-scale compared with instantaneous mixing, which produced narrow spectra. Su *et al.* (1998) found that the limiting case of mixing by molecular diffusion alone produced the broadest spectra. In the context of LES, a subgrid model for filamentation has been developed by Grabowski (2007) and Jarecka *et al.* (2009) drawing on developments in combustion modelling.

Grabowski (2007) proposed an advection–diffusion equation for the length scale, λ, of a filament based on the similarity arguments of Broadwell and Breidenthal (1982), who suggested that filaments of a conserved scalar field should obey

$$\frac{d\lambda}{dt} = -\alpha \varepsilon^{1/3} \lambda^{1/3}, \qquad (15)$$

where α is a constant. The advection–diffusion equation for λ includes a forcing term of the same form as the right-hand side of (15) and a source–sink term which resets λ to the grid scale or zero depending on whether cloudy air forms as a result of grid-scale condensation, complete evaporation of the grid-scale cloudy air occurs or there is homogenization of a cloudy volume. The coupling of this equation to the governing LES equations and the application of this model to shallow cumulus shows a significant impact on mean liquid water path, cloud depth and cloud water content when the grid spacing is large (Grabowski, 2007). This model was extended by Jarecka *et al.* (2009) to include an advection–diffusion equation for the fraction of grid box with cloudy air, β. The addition of a prognostic equation for β did not result in significant changes to the mean cloud properties but, by allowing a local diagnosis of the homogeneity of the mixing process, does indicate a method for predicting changes to the droplet size spectrum as a result of entrainment. Grabowski (2007) noted a considerable sensitivity to the value of α and, although theoretical arguments based on linear-eddy modelling suggest that $\alpha \approx 1.8$, more detailed simulations, especially DNS, are required to provide a reliable estimate of this parameter.

The effect of off-source heating on entrainment in a turbulent jet has been studied in both laboratory experiments (e.g. Elavarasan *et al.*, 1995; Bhat and Narasimha, 1996; Agrawal and Prasad, 2004) and numerical simulations (e.g. Basu and Narasimha, 1999; Agrawal *et al.*, 2004). Here, additional energy is injected into a well-developed jet far from the source and over a finite streamwise extent. The results indicate that off-source heating disrupts the large-scale eddies and so decreases the entrainment rate. However, the precise mechanisms are complicated and vary within the region of off-source heating (Agrawal and Prasad, 2004). Since off-source heating may mimic latent heating, these results have been used as a basis for explaining why lateral entrainment rates in cumulus clouds have sometimes been observed to be low. However, as pointed out in section 2.2.1, cumulus clouds are characterized by a descending shell of negative buoyancy which could impact on the entrainment rate.

The entrainment interfacial layer that characterizes the top of stratocumulus clouds plays a similar role to the descending shell in cumulus clouds. Although the dynamics in the two cases may be very different, it suggests that a layer containing air of more than one origin may play an important role in entraining dry air into a cloud. It is also a distinguishing feature of turbulent clouds that does not occur in laboratory jets or plumes. A detailed study of the cloud-top structure of stratocumulus by Moeng *et al.* (2005) led to the question: where is the interface and which interface should be considered as the interface through which mixing occurs? These questions have been addressed by Kurowski *et al.* (2009), who followed passive tracers in LES of stratocumulus. Their simulations confirm the existence of an entrainment interfacial layer and show that only a small fraction of air undergoing mixing at the cloud top, in proportions which are just right to produce negative buoyancy, sinks down into the cloud layer. The complexity of the mixing and entrainment processes at the top of stratocumulus has motivated the application of level-set methods used in the study of combustion to study entrainment and mixing in idealized models of stratocumulus. The level-set method is a computational technique for tracking propagating interfaces, for which the interface is described by a single non-reacting scalar

equation (see, for example, Peters, 2000, sections 2.5–2.8). An example of its application to the cloud–clear air interface is described next.

Mellado *et al.* (2009) consider two unbounded fluids: a warmer subsaturated fluid above a cooler supersaturated one with gravity directed downwards and an advection–diffusion equation for the mixture fraction. They characterize the results of their two-dimensional simulations in terms of a buoyancy reversal parameter, D, introduced by Siems *et al.* (1990) and Shy and Breidenthal (1990) and defined to be the ratio of maximum density change of the mixture (relative to the lower fluid) to the density difference of the unmixed fluids. Buoyancy reversal occurs when $D > 0$ and a critical value for instability is thought to be of order unity (Siems *et al.*, 1990). Realistic cloud-top conditions typically have $D \ll 1$ and this limit is the focus of Mellado *et al.* (2009). A linear stability analysis by Mellado *et al.* (2009) leads naturally to the condition $D > 0$ required for buoyancy reversal and showed that the system sustains an unstable mode. The authors provide another interpretation of $\sqrt{D}$ as the ratio of the time-scale of the (equilibrium) restoring force of the density interface to the time-scale of the unstable downdraught. Since $D \ll 1$ the system returns to equilibrium faster than a mixture with negative buoyancy is able to descend; the turbulence within the cloud is too weak to destabilize the inversion, which could in turn break up the cloud layer and is consistent with a large (convection-scale) Richardson number that also increases with time. Three-dimensional simulations by Mellado (2010) support these arguments: they find that convoluted flow patterns can be generated by evaporative cooling even for $D \ll 1$ but that there is no enhanced entrainment of upper fluid in the absence of shear. Indeed, they find that the rate of mixing with the upper layer is limited by the molecular diffusivity, which constrains the rate at which a convective layer can develop below the inversion. The simulations of Mellado (2010) show that buoyancy reversal is a consequence of molecular mixing with the upper layer, which in turn leads to a turbulent state in the lower layer, but that buoyancy reversal alone does not lead to the break-up of the inversion. Their results show that the enhancement of turbulent mixing by evaporative cooling is restricted to the lower layer. These results support earlier results (e.g. Shy and Breidenthal, 1990; Siems *et al.*, 1990) that buoyancy reversal alone is not sufficient to destabilize stratocumulus.

As mentioned at the beginning of this section, entrainment is usually characterized as a three-stage process in which the initial engulfment of dry air is followed by a process of filamentation (stirring) and finally diffusion or mixing at the viscous scale (e.g. Eckart, 1948; Dimotakis, 1986; Dimotakis, 2005). Entrainment has also been characterized as 'nibbling': the diffusion of irrotational ambient air into the turbulent fluid (e.g. Corrsin and Kistler, 1955; Dimotakis, 1986). The terms 'engulfment' and 'nibbling' have also been used more loosely to describe essentially large-scale or small-scale motions respectively. Laboratory experiments (Westerweel *et al.*, 2009) and numerical simulations (Mathew and Basu, 2002) of entrainment by a turbulent jet both show that the dominant process is nibbling rather than engulfing, although neither the experiments nor the simulations had the wide range of scales typical of real clouds. Because this entrainment process extends only over a limited distance,

there is very little unmixed external fluid in the interior of the jet (Westerweel *et al.*, 2009). When additional turbulence is generated within the plume or jet, such as would result from latent heating, it has been speculated that engulfment may become more important (Westerweel *et al.*, 2009). Indeed, dry air may penetrate the core of a cumulus cloud in so far as this picture of entrainment and mixing in cumulus is valid. In their laboratory experiments on mixing across a density interface, Shy and Breidenthal (1990) note that engulfment only occurs when $D \geqslant 1.3$, whereas nibbling is apparently negligible in this case. For $D < 1.3$ the reverse is true. The results of Mellado *et al.* (2009) appear to support this finding, indicating that perhaps molecular diffusion is the dominant mechanism for entrainment in stratocumulus clouds (although ambient shear may change this picture). The conceptual view of entrainment as either engulfment or nibbling may be oversimplified but, in the context of cumulus and stratocumulus, could merit further attention, especially as there are indications that the dominant entrainment processes differ in the two cloud types. Whether entrainment is primarily engulfing or nibbling may impact on the nature of the mixing process and the droplet size distribution, particularly how far broadening of the droplet size distribution by entrainment extends into the core of cumulus clouds or well below the top of stratocumulus.

6. Conclusions

This survey has shown that turbulence plays a significant and widespread role in the process of cloud formation. Clouds are an example of a naturally occurring turbulent multiphase flow: warm clouds are a turbulent suspension of droplets that exhibit strong aerodynamic and thermodynamic inter-phase couplings (Bodenschatz *et al.*, 2010). They share many similarities with other geophysical and engineering flows, yet also differences that need to be appreciated when extrapolating the results of simplified models to real clouds. The importance of sedimentation is an obvious example, as is the importance of latent heating in cloud dynamics. Nevertheless, this survey has shown that significant improvements in the understanding of cloud processes can be made by studying relatively simple models even if they do not capture all aspects of clouds. Despite the obvious difficulties, much progress has been made theoretically in recent years, such as a derivation of the collision kernel for finite St. However, it remains a formidable challenge to extend these approaches to more realistic situations, even just the anisotropy introduced by gravity. Similarly, as remarked by Khain *et al.* (2007), a rigorous averaging of the stochastic coalescence equation that takes into account differential sedimentation remains an open problem. It is thus likely that numerical simulations and laboratory experiments will offer much valuable insight in the foreseeable future.

DNS has been used extensively to study cloud-like processes despite its limited range of scales. By focusing on parameter ranges which are relevant to clouds, such as appropriate values of ε and bidisperse suspensions of droplets, it has been possible, for example, to deduce the relative contributions to the turbulent enhancement of the collision kernel from the relative velocity of the droplets, droplet clustering and collision efficiency. Of course, the extension of these models to higher Reynolds numbers is not guaranteed since the range of relevant values of

parameters such as St and Sv may grow. This highlights the lack of a theoretical framework for constructing the R_λ-dependence of the turbulent collision kernel and makes it difficult to assess the validity of parametrizations derived from DNS particularly when used in more realistic models of clouds such as LES. These limitations mean that the effects of turbulence on cloud formation, such as the importance of droplet clustering, are likely to remain controversial for some time to come. The lack of observations of real clouds at the smallest scales that can simultaneously measure the statistics of the flow (turbulence), the scalar fields (thermodynamics) and the droplets (microphysics) compounds these limitations. However, recent observations at centimetre scales and the 3-D statistics that can be obtained with holographic cameras offer grounds for encouragement.

This survey indicates many areas where there is scope for further simulations and laboratory experiments: a wider range of St, Sv and Fr_p values should be considered as computers become more powerful and laboratory experiments improve. The relative importance of local *versus* long-range effects is still uncertain: more research is required on the role of caustics, particularly their Reynolds number dependence, and there is scope for developing parametrizations of the collision kernel that combine both these effects. As discussed in this survey, there still remains much debate over the relative importance of processes such as entrainment and mixing and the small-scale processes that affect the turbulent collision kernel. An example of the potential complexity was remarked upon by Lehmann *et al.* (2007): the higher dissipation rates that are typically found at cloud edges could increase the collision rate via enhanced clustering because of higher values of St at the same time as entrainment reduces the droplet number density and hence the collision rate. However, the processes involved are not necessarily competing since mixing due to entrainment is associated with the inertial subrange of turbulence, whereas droplet clustering as discussed in section 4.2.2.2 is associated with the viscous dissipation range (with the caveat mentioned throughout this survey that all scales of turbulence affect the statistics of even the smallest scales). Nevertheless, there is much scope here for a range of studies from DNS of idealized interfacial flows with and without droplets to LES with refined subgrid models of droplet microphysics. Such simulations may be expensive now but increasing computer power will make them more feasible in the future.

In this survey, we have reviewed the very diverse processes that contribute to droplet growth and rain formation in warm clouds, from the cloud scale to the microscale. These concepts and theories have been developed to explain how convective clouds can precipitate in a short time. Surprisingly, the time it takes for a cloud to precipitate is one of the least certain parameters in cloud physics. Observations are common with cloud radars, but clouds only start to become visible with a radar once a few raindrops have already formed. Innovative strategies are needed to detect clouds at their inception and to follow them until precipitation starts in order to quantitatively assess the ubiquitous, though unclear, statement that warm clouds are precipitating faster than expected.

List of principal symbols

a Droplet radius
f Droplet size distribution or spectral density function
g_{12} Radial distribution function
n Droplet number concentration per unit volume
r_c Collision radius: $r_c = a_1 + a_2$
s Supersaturation
s_{qe} Quasi-equilibrium value of s
$\boldsymbol{u}$ Velocity of air
$\boldsymbol{v}_p$ Droplet velocity
w Vertical component of $\boldsymbol{u}$
w_r Longitudinal relative velocity component of two droplets
Da Damköhler number: $\mathrm{Da} = \tau_r/\tau_s$
E_{12} Collision efficiency
Fr_f Froude number of fluid: $\mathrm{Fr}_f = v_\eta^2/(g\eta)$
Fr_p Froude number of particle: $\mathrm{Fr}_p = St^3/\mathrm{Fr}_f^2$
$\mathcal{N}_{12}$ Geometric collision rate per unit volume
R_λ Taylor-scale Reynolds number
St Stokes number: $\mathrm{St} = \tau_p/\tau_\eta$
Sv Non-dimensional terminal velocity: $\mathrm{Sv} = v_T/v_\eta = \tau_\eta/\tau_v$
v_T Droplet terminal velocity: $v_T = g\tau_p$
v_η Kolmogorov velocity scale
ε Mean kinetic energy dissipation rate
η Kolmogorov length scale
ρ_a Density of air
ρ_w Density of liquid water
τ_p Droplet response time
τ_r Time-scale of a turbulent eddy of scale r: $\tau_r \sim r^{2/3}/\varepsilon^{1/3}$
τ_η Kolmogorov time-scale
τ_s Phase relaxation time-scale
τ_v Sedimentation time-scale
Γ_{12} Collision kernel

References

Abrahamson J. 1975. Collision rates of small particles in a vigorously turbulent fluid. *J. Chem. Eng. Sci.* **30**: 1371–1379.

Agrawal A, Prasad AK. 2004. Evolution of a turbulent jet subjected to volumetric heating. *J. Fluid Mech.* **511**: 95–123.

Agrawal A, Boersma BJ, Prasad AK. 2004. Direct numerical simulation of a turbulent axisymmetric jet with buoyancy-induced acceleration. *Flow Turb. Combust.* **73**: 277–305.

Aliseda A, Cartellier A, Hainaux F, Lasheras JC. 2002. Effect of preferential concentration on the settling velocity of heavy particles in homogeneous isotropic turbulence. *J. Fluid Mech.* **468**: 77–105.

Ammar Y, Reeks MW. 2009. Agglomeration of inertial particles in a random rotating symmetric straining flow. *Int. J. Multiphase Flow* **35**: 840–853.

Andrejczuk M, Grabowski WW, Malinowski SP, Smolarkiewicz PK. 2004. Numerical simulation of cloud–clear air interfacial mixing. *J. Atmos. Sci.* **61**: 1726–1739.

Andrejczuk M, Grabowski WW, Malinowski SP, Smolarkiewicz PK. 2006. Numerical simulation of cloud–clear air interfacial mixing: effects of cloud microphysics. *J. Atmos. Sci.* **63**: 3204–3225.

Andrejczuk M, Reisner JM, Henson B, Dubey MK, Jeffery CA. 2008. The potential impacts of pollution on a nondrizzling stratus deck: does aerosol number matter more than type? *J. Geophys. Res.* **113**: D19204, DOI: 10.1029/2007JD009445.

Andrejczuk M, Grabowski WW, Malinowski SP, Smolarkiewicz PK. 2009. Numerical simulation of cloud–clear air interfacial mixing: homogeneous versus inhomogeneous mixing. *J. Atmos. Sci.* **66**: 2493–2500.

Andrejczuk M, Grabowski WW, Reisner J, Gadian A. 2010. Cloud–aerosol interactions for boundary layer stratocumulus in the Lagrangian Cloud Model. *J. Geophys. Res.* **115**: D22214, DOI: 10.1029/2010JD014248.

Arabas S, Pawlowska H, Grabowski WW. 2009. Effective radius and droplet spectral width from in-situ aircraft observations in trade-wind cumuli during RICO. *Geophys. Res. Lett.* **36**: L11803, DOI: 10.1029/2009GL038257.

Ayala O, Rosa B, Wang L-P, Grabowski WW. 2008a. Effects of turbulence on the geometric collision rate of sedimenting droplets. Part 1. Results from direct numerical simulation. *New J. Phys.* **10**: 075015, DOI: 10.1088/1367-2630/10/7/075015.

Ayala O, Rosa B, Wang L-P. 2008b. Effects of turbulence on the geometric collision rate of sedimenting droplets. Part 2. Theory and parameterization. *New J. Phys.* **10**: 075016, DOI: 10.1088/1367-2630/10/7/075016.

Ayyalasomayajula S, Gylfason A, Collins LR, Bodenschatz E, Warhaft Z. 2006. Lagrangian measurements of inertial particle accelerations in grid generated wind tunnel turbulence. *Phys. Rev. Lett.* **97**: 144507, DOI: 10.1017/S0022112008004187.

Ayyalasomayajula S, Warhaft Z, Collins LR. 2008. Modeling inertial particle statistics in isotropic turbulence. *Phys. Fluids* **20**: 095104, DOI: 10.1063/1.2976174.

Baker BA. 1992. Turbulent entrainment and mixing in clouds: a new observational approach. *J. Atmos. Sci.* **49**: 387–404.

Baker BA, Lawson RP. 2010. Analysis of tools used to quantify droplet clustering in clouds. *J. Atmos. Sci.* **67**: 3355–3367.

Baker MB, Latham J. 1979. The evolution of droplet spectra and the rate of production of embryonic raindrops in small cumulus clouds. *J. Atmos. Sci.* **36**: 1612–1615.

Baker MB, Corbin RG, Latham J. 1980. The influence of entrainment on the evolution of cloud droplet spectra: I. A model of inhomogeneous mixing. *Q. J. R. Meteorol. Soc.* **106**: 581–598.

Balkovsky E, Falkovich G, Fouxon A. 2001. Intermittent distribution of inertial particles in turbulent flows. *Phys. Rev. Lett.* **86**: 2790–2793.

Basu AJ, Narasimha R. 1999. Direct numerical simulation of turbulent flows with cloud-like off-source heating. *J. Fluid Mech.* **385**: 199–228.

Batchelor GK. 1967. *An Introduction to Fluid Dynamics*. Cambridge University Press: Cambridge, UK.

Beard KV. 1976. Terminal velocity and shape of cloud and precipitation drops aloft. *J. Atmos. Sci.* **33**: 851–864.

Bec J. 2005. Multifractal concentrations of inertial particles in smooth random flows. *J. Fluid Mech.* **528**: 255–277.

Bec J, Biferale L, Boffetta G, Celani A, Cencini M, Lanotte A, Musacchio S, Toschi F. 2006. Acceleration statistics of heavy particles in turbulence. *J. Fluid Mech.* **550**: 349–358.

Bec J, Biferale L, Cencini M, Lanotte A, Musacchio S, Toschi F. 2007. Heavy particle concentration in turbulence at dissipative and inertial scales. *Phys. Rev. Lett.* **98**: 084502, DOI: 10.1103/PhysRevLett.98.084502.

Bhat GS, Narasimha R. 1996. A volumetrically heated jet: large-eddy structure and entrainment characteristics. *J. Fluid Mech.* **325**: 303–330.

Blyth AM. 1993. Entrainment in cumulus clouds. *J. Appl. Meteorol.* **32**: 626–641.

Blyth AM, Cooper WA, Jensen JB. 1988. A study of the source of entrained air in Montana cumuli. *J. Atmos. Sci.* **45**: 3944–3964.

Bodenschatz E, Malinowski SP, Shaw RA, Stratmann F. 2010. Can we understand clouds without turbulence? *Science* **327**: 970–971.

Boers R, Jensen JB, Krummel PB. 1998. Microphysical and short-wave radiative structure of stratocumulus clouds over the Southern Ocean: summer results and seasonal differences. *Q. J. R. Meteorol. Soc.* **124**: 151–168.

Brenguier J-L, Chaumat L. 2001. Droplet spectra broadening in cumulus clouds. Part I: Broadening in adiabatic cores. *J. Atmos. Sci.* **58**: 628–641.

Brenguier J-L, Grabowski WW. 1993. Cumulus entrainment and cloud droplet spectra: a numerical model within a two-dimensional dynamical framework. *J. Atmos. Sci.* **50**: 120–136.

Brenguier J-L, Bourrianne T, de Araujo Coelho A, Isbert J, Peytavi R, Trevarin D, Weschler P. 1998. Improvements of droplet size distribution measurements with the Fast-FSSP (Forward Scattering Spectrometer Probe). *J. Atmos. Ocean. Technol.* **15**: 1077–1090.

Broadwell JE, Breidenthal RE. 1982. A simple model of mixing and chemical reaction in a turbulent shear layer. *J. Fluid Mech.* **125**: 397–410.

Brooke JW, Hanratty TJ, McLaughlin JB. 1994. Free-flight mixing and deposition of aerosols. *Phys. Fluids* **6**: 3404–3415.

Burnet F, Brenguier J-L. 2007. Observational study of the entrainment-mixing process in warm convective clouds. *J. Atmos. Sci.* **64**: 1995–2011.

Caughey SJ, Crease BA, Roach WT. 1982. A field study of nocturnal stratocumulus. II. Turbulence structure and entrainment. *Q. J. R. Meteorol. Soc.* **108**: 125–144.

Celani A, Falkovich G, Mazzino A, Seminara A. 2005. Droplet condensation in turbulent flows. *Europhys. Lett.* **70**: 775–781.

Celani A, Mazzino A, Seminara A, Tizzi M. 2007. Droplet condensation in two-dimensional Bolgiano turbulence. *J. Turb.* **8**: N17.

Chaumat L, Brenguier J-L. 2001. Droplet spectra broadening in cumulus clouds. Part II: Microscale droplet concentration heterogeneities. *J. Atmos. Sci.* **58**: 642–654.

Chun J, Koch DL, Rani SL, Ahluwalia A, Collins LR. 2005. Clustering of aerosol particles in isotropic turbulence. *J. Fluid Mech.* **536**: 219–251.

Coleman SW, Vassilicos JC. 2009. A unified sweep-stick mechanism to explain particle clustering in 2- and 3-dimensional homogeneous, isotropic turbulence. *Phys. Fluids* **21**: 113301, DOI: 10.1063/1.3257638.

Cooper WA. 1989. Effects of variable droplet growth histories on droplet size distributions. Part I: Theory. *J. Atmos. Sci.* **46**: 1301–1311.

Corrsin S, Kistler AL. 1955. Free-stream boundaries of turbulent flows. *NACA Report 1244*.

Csanady GT. 1963. Turbulent diffusion of heavy particles in the atmosphere. *J. Atmos. Sci.* **20**: 201–208.

Dallas V, Vassilicos JC. 2011. Rapid growth of cloud droplets by turbulence. *Phys. Rev. E* **84**: 046315, DOI: 10.1103/PhysRevE.84.046315.

Dávila J, Hunt JCR. 2001. Settling of small particles near vortices and in turbulence. *J. Fluid Mech.* **440**: 117–145.

Deardorff JW. 1980. Cloud top entrainment instability. *J. Atmos. Sci.* **37**: 131–147.

de Jong J, Salazar JPLC, Woodward SH, Collins LR, Meng H. 2010. Measurement of inertial particle clustering and relative velocity statistics in isotropic turbulence using holographic imaging. *Int. J. Multiphase Flow* **36**: 324–332.

Dimotakis PE. 1986. Two-dimensional shear-layer entrainment. *AIAA J.* **24**: 1791–1796.

Dimotakis PE. 2005. Turbulent mixing. *Annu. Rev. Fluid Mech.* **37**: 329–356.

Dodin Z, Elperin T. 2002. On the collision rate of particles in turbulent flow with gravity. *Phys. Fluids* **14**: 2921–2924.

Ducasse L, Pumir A. 2009. Inertial particle collisions in turbulent synthetic flows: quantifying the sling effect. *Phys. Rev. E* **80**: 066312, DOI: 10.1103/PhysRevE.80.066312.

Dye JE, Baumgardner D. 1984. Evaluation of the Forward Scattering Spectrometer Probe. Part I: Electronic and optical studies. *J. Atmos. Ocean. Technol.* **1**: 329–344.

Eckart C. 1948. An analysis of the stirring and mixing processes in incompressible fluids. *J. Mar. Res.* **7**: 265–275.

Elavarasan R, Bhat GS, Prabhu A, Narasimha R. 1995. An experimental study of a jet with local buoyancy enhancement. *Fluid Dyn. Res.* **16**: 189–202.

Elghobashi S. 1994. On predicting particle-laden turbulent flows. *Appl. Sci. Res* **52**: 309–329.

Falkovich G, Pumir A. 2004. Intermittent distribution of heavy particles in a turbulent flow. *Phys. Fluids* **16**: L47–L50.

Falkovich G, Pumir A. 2007. Sling effect in collisions of water droplets in turbulent clouds. *J. Atmos. Sci.* **64**: 4497–4505.

Falkovich G, Fouxon A, Stepanov MG. 2002. Acceleration of rain initiation by cloud turbulence. *Nature* **419**: 151–154.

Feingold G, Kreidenweis SM, Zhang Y. 1998. Stratocumulus processing of gases and cloud condensation nuclei. 1. Trajectory ensemble model. *J. Geophys. Res.* **103**: 19527–19542.

Février P, Simonin O, Squires KD. 2005. Partitioning of particle velocities in gas–solid turbulent flows into a continuous field and a spatially uncorrelated random distribution: theoretical formalism and numerical study. *J. Fluid Mech.* **553**: 1–46.

Franklin CN. 2008. A warm rain microphysics parameterization that includes the effect of turbulence. *J. Atmos. Sci.* **65**: 1795–1816.

Franklin CN, Vaillancourt PA, Yau MK. 2007. Statistics and parameterizations of the effect of turbulence on the geometric collision kernel of cloud droplets. *J. Atmos. Sci.* **64**: 938–954.

Fukuta N. 1992. Theories of competitive cloud droplet growth and their application to cloud physics studies. *J. Atmos. Sci.* **49**: 1107–1114.

Fung JCH, Hunt JCR, Malik NA, Perkins RJ. 1992. Kinematic simulation of homogeneous turbulence by unsteady random Fourier modes. *J. Fluid Mech.* **236**: 281–318.

Gerashchenko S, Good G, Warhaft Z. 2011. Entrainment and mixing of water droplets across a shearless turbulent interface with and without gravitational effects. *J. Fluid Mech.* **668**: 293–303.

Gerber H. 1996. Microphysics of marine stratocumulus clouds with two drizzle modes. *J. Atmos. Sci.* **53**: 1649–1662.

Gerber H, Frick G, Malinowski SP, Brenguier J-L, Burnet F. 2005. Holes and entrainment in stratocumulus. *J. Atmos. Sci.* **62**: 443–459.

Gerber HE, Frick GM, Jensen JB, Hudson JG. 2008. Entrainment, mixing, and microphysics in trade-wind cumulus. *J. Met. Soc. Japan* **86A**: 87–106.

Ghosh S, Jonas PR. 2001. Some analytical calculations on the effect of turbulence on the settling and growth of cloud droplets. *Geophys. Res. Lett.* **28**: 3883–3886.

Ghosh S, Dávila J, Hunt JCR, Srdic A, Fernando HJS, Jonas PR. 2005. How turbulence enhances coalescence of settling particles with applications to rain in clouds. *Proc. R. Soc. A* **461**: 3059–3088.

Good GH, Gerashchenko S, Warhaft Z. 2012. Intermittency and inertial particle entrainment at a turbulent interface: the effect of the large-scale eddies. *J. Fluid Mech.* DOI: 10.1017/jfm.2011.552.

Goto S, Vassilicos JC. 2006. Self-similar clustering of inertial particles and zero-acceleration points in fully developed two-dimensional turbulence. *Phys. Fluids* **18**: 115103, DOI: 10.1063/1.2364263.

Grabowski WW. 2000. Dynamics of cumulus entrainment. In *Geophysical and Astrophysical Convection*, Kerr R, Fox P (eds). Gordon & Breach: Amsterdam; 107–127.

Grabowski WW. 2007. Representation of turbulent mixing and buoyancy reversal in bulk cloud models. *J. Atmos. Sci.* **64**: 3666–3680.

Grabowski WW, Clark TL. 1991. Cloud–environment interface instability: rising thermal calculations in two spatial dimensions. *J. Atmos. Sci.* **48**: 527–546.

Grabowski WW, Clark TL. 1993a. Cloud–environment interface instability. Part II: Extension to three spatial dimensions. *J. Atmos. Sci.* **50**: 555–573.

Grabowski WW, Clark TL. 1993b. Cloud–environment interface instability. Part III: Direct influence of environmental shear. *J. Atmos. Sci.* **50**: 3821–3828.

Grabowski WW, Vaillancourt P. 1999. Comments on 'Preferential concentration of cloud droplets by turbulence: effects on the early evolution of cumulus cloud droplet spectra'. *J. Atmos. Sci.* **56**: 1433–1436.

Grabowski WW, Wang L-P. 2009. Diffusional and accretional growth of water drops in a rising adiabatic parcel: effects of the turbulent collision kernel. *Atmos. Chem. Phys.* **9**: 2335–2353.

Haman KE, Malinowski SP, Kurowski MJ, Gerber H, Brenguier J-L. 2007. Small-scale mixing processes at the top of a marine stratocumulus: a case-study. *Q. J. R. Meteorol. Soc.* **133**: 213–226.

Heus T, Jonker HJJ. 2008. Subsiding shells around shallow cumulus clouds. *J. Atmos. Sci.* **65**: 1003–1018.

Heus T, van Dijk G, Jonker HJJ, van den Akker HEA. 2008. Mixing in shallow cumulus studied by Lagrangian particle tracking. *J. Atmos. Sci.* **65**: 2581–2597.

Holtzer GL, Collins LR. 2002. Relationship between the intrinsic radial distribution function for an isotropic field of particles and lower-dimensional measurements. *J. Fluid Mech.* **459**: 93–102.

Hsieh WC, Jonsson H, Wang L-P, Buzorius G, Flagan RC, Seinfeld JH, Nenes A. 2009. On the representation of droplet coalescence and autoconversion: evaluation using ambient cloud droplet size distributions. *J. Geophys. Res.* **114**: D07201, DOI: 10.1029/2008JD010502.

IJzermans RHA, Reeks MW, Meneguz E, Picciotto M, Soldati A. 2009. Measuring segregation of inertial particles in turbulence by a full Lagrangian approach. *Phys. Rev. E* **80**: 015302, DOI: 10.1103/PhysRevE.80.015302.

IJzermans RHA, Meneguz E, Reeks MW. 2010. Segregation of particles in incompressible random flows: singularities, intermittency and random uncorrelated motion. *J. Fluid Mech.* **653**: 99–136.

Jaczewski A, Malinowski SP. 2005. Spatial distribution of cloud droplets in a turbulent cloud-chamber flow. *Q. J. R. Meteorol. Soc.* **131**: 2047–2062.

Jarecka D, Grabowski WW, Pawlowska H. 2009. Modeling of subgrid-scale mixing in large-eddy simulation of shallow convection. *J. Atmos. Sci.* **66**: 2125–2133.

Jeffery CA. 2007. Inhomogeneous cloud evaporation, invariance and Damköhler number. *J. Geophys. Res.* **112**: D24S21, DOI: 10.1029/2007JD008789.

Jeffery CA, Reisner JM. 2006. A study of cloud mixing and evolution using pdf methods. Part I: Cloud front propagation and evaporation. *J. Atmos. Sci.* **63**: 2848–2864.

Jennings SG. 1988. The mean free path in air. *J. Aerosol Sci.* **19**: 159–166.

Jiang H, Feingold G, Jonsson HH, Lu M-L, Chuang PY, Flagan RC, Seinfeld JH. 2008. Statistical comparison of properties of simulated and observed cumulus clouds in the vicinity of Houston during the Gulf of Mexico Atmospheric Composition and Climate Study (GoMACCS). *J. Geophys. Res.* **113**: D13205, DOI: 10.1029/2007JD009304.

Jonas PR. 1990. Observations of cumulus cloud entrainment. *Atmos. Res.* **25**: 105–127.

Kerstein AR, Krueger SK. 2006. Clustering of randomly advected low inertia particles: a solvable model. *Phys. Rev. E* **73**: 025302, DOI: 10.1103/PhysRevE.73.025302.

Khain A, Pinsky M, Elperin T, Kleeorin N, Rogachevskii I, Kostinski A. 2007. Critical comments to results of investigations of drop collisions in turbulent clouds. *Atmos. Res.* **86**: 1–20.

Khvorostyanov VI, Curry JA. 1999. Toward the theory of stochastic condensation in clouds. Part I: A general kinetic equation. *J. Atmos. Sci.* **56**: 3985–3996.

Klaassen GP, Clark TL. 1985. Dynamics of the cloud-environment interface and entrainment in small cumuli: two-dimensional simulations in the absence of ambient shear. *J. Atmos. Sci.* **42**: 2621–2642.

Korolev AV, Mazin IP. 2003. Supersaturation of water vapor in clouds. *J. Atmos. Sci.* **60**: 2957–2974.

Kostinski AB. 2009. Simple approximations for condensational growth. *Env. Res. Lett.* **4**: 015005, DOI: 10.1088/1748-9326/4/1/015005.

Kostinski AB, Shaw RA. 2001. Scale-dependent droplet clustering in turbulent clouds. *J. Fluid Mech.* **434**: 389–398.

Kostinski AB, Shaw RA. 2005. Fluctuations and luck in droplet growth by coalescence. *Bull. Am. Meteorol. Soc.* **86**: 235–244.

Krueger SK. 1993. Linear eddy modeling of entrainment and mixing in stratus clouds. *J. Atmos. Sci.* **50**: 3078–3090.

Krueger SK, Su C-W, McMurtry PA. 1997. Modeling entrainment and finescale mixing in cumulus clouds. *J. Atmos. Sci.* **54**: 2697–2712.

Kuo H-C, Schubert WH. 1988. Stability of cloud-topped boundary layers. *Q. J. R. Meteorol. Soc.* **114**: 887–916.

Kurowski MJ, Malinowski SP, Grabowski WW. 2009. A numerical investigation of entrainment and transport within a stratocumulus-topped boundary layer. *Q. J. R. Meteorol. Soc.* **135**: 77–92.

Lanotte AS, Seminara A, Toschi F. 2009. Cloud droplet growth by condensation in homogeneous isotropic turbulence. *J. Atmos. Sci.* **66**: 1685–1697.

Lasher-Trapp SG, Cooper WA, Blyth AM. 2005. Broadening of droplet size distributions from entrainment and mixing in a cumulus cloud. *Q. J. R. Meteorol. Soc.* **131**: 195–220.

Latham J, Reed RL. 1977. Laboratory studies of the effects of mixing on the evolution of cloud droplet spectra. *Q. J. R. Meteorol. Soc.* **103**: 297–306.

Lau KM, Wu HT. 2003. Warm rain processes over tropical oceans and climate implications. *Geophys. Res. Lett.* **30**: 2290, DOI: 10.1029/2003GL018567.

Lehmann K, Siebert H, Wendisch M, Shaw RA. 2007. Evidence for inertial droplet clustering in weakly turbulent clouds. *Tellus B* **59**: 57–65.

Lehmann K, Siebert H, Shaw RA. 2009. Homogeneous and inhomogeneous mixing in cumulus clouds: dependence on local turbulence structure. *J. Atmos. Sci.* **66**: 3641–3659.

Lin YJP, Linden PF. 2005. The entrainment due to a turbulent fountain at a density interface. *J. Fluid Mech.* **542**: 25–52.

Lu J, Nordsiek H, Shaw RA. 2010. Clustering of settling charged particles in turbulence: theory and experiments. *New J. Phys.* **12**: 123030, DOI: 10.1088/1367-2630/12/12/123030.

MacPherson JI, Isaac GA. 1977. Turbulent characteristics of some Canadian cumulus clouds. *J. Appl. Met.* **16**: 81–90.

Magaritz L, Pinsky M, Krasnov O, Khain A. 2009. Investigation of droplet size distributions and drizzle formation using a new trajectory ensemble model. Part II: Lucky parcels. *J. Atmos. Sci.* **66**: 781–805.

Mahrt L. 1979. Penetrative convection at the top of a growing boundary layer. *Q. J. R. Meteorol. Soc.* **105**: 469–485.

Malinowski SP, Andrejczuk M, Grabowski WW, Korczyk P, Kowalewski TA, Smolarkiewicz PK. 2008. Laboratory and modeling studies of cloud-clear air interfacial mixing: anisotropy of small-scale turbulence due to evaporative cooling. *New J. Phys.* **10**: 075020, DOI: 10.1088/1367-2630/10/7/075020.

Masi E, Riber E, Sierra P, Simonin O, Gicquel LYM. 2010. Modeling the random uncorrelated velocity stress tensor for unsteady particle Eulerian simulation in turbulent flows. In *7th International Conference on Multiphase Flow (ICMF 2010)*, Tampa, FL.

Mason BJ. 1971. *The Physics of Clouds*. Oxford University Press: Oxford.

Mathew J, Basu A. 2002. Some characteristics of entrainment at a cylindrical turbulence boundary. *Phys. Fluids* **14**: 2065–2072.

Maxey MR. 1987. The gravitational settling of aerosol particles in homogeneous turbulence and random flow fields. *J. Fluid Mech.* **174**: 441–465.

Maxey MR, Riley JJ. 1983. Equation of motion for a small rigid sphere in a nonuniform flow. *Phys. Fluids* **26**: 883–889.

Meischner P, Baumann R, Höller H, Jank T. 2001. Eddy dissipation rates in thunderstorms estimated by Doppler radar in relation to aircraft in situ measurements. *J. Atmos. Ocean. Technol.* **18**: 1609–1627.

Mellado JP. 2010. The evaporatively driven cloud-top mixing layer. *J. Fluid Mech.* **660**: 5–36.

Mellado JP, Stevens B, Schmidt H, Peters N. 2009. Buoyancy reversal in cloud-top mixing layers. *Q. J. R. Meteorol. Soc.* **135**: 963–978.

Meneguz EM, Reeks MW. 2010. A Lagrangian approach for quantifying the segregation of inertial particles in incompressible turbulent flows. In *7th International Conference on Multiphase Flow (ICMF 2010)*, Tampa, FL.

Meneguz E, Reeks MW. 2011. Statistical properties of particle segregation in homogeneous isotropic turbulence. *J. Fluid Mech.* **686**: 338–351.

Miao Q, Geerts B, LeMone M. 2006. Vertical velocity and buoyancy characteristics of coherent echo plumes in the convective boundary layer, detected by a profiling airborne radar. *J. Appl. Meteorol. Climatol.* **45**: 838–855.

Moeng C-H, Stevens B, Sullivan PP. 2005. Where is the interface of the stratocumulus-topped PBL? *J. Atmos. Sci.* **62**: 2626–2631.

Monchaux R, Bourgoin M, Cartellier A. 2010. Preferential concentration of heavy particles: a Voronoi analysis. *Phys. Fluids* **22**: 103304, DOI: 10.1063/1.3489987.

Monin AS, Yaglom AM. 1975. *Statistical Fluid Mechanics*, Vol. 2. MIT Press: Cambridge, MA.

Morton BR. 1957. Buoyant plumes in a moist atmosphere. *J. Fluid Mech.* **2**: 127–144.

Morton BR, Taylor G, Turner JS. 1956. Turbulent gravitational convection from maintained and instantaneous sources. *Proc. R. Soc. A* **234**: 1–23.

Nielsen P. 1993. Turbulence effects on the settling of suspended particles. *J. Sediment. Petrol.* **63**: 835–838.

Onishi R, Takahashi K, Komori S. 2009. Influence of gravity on collisions of monodisperse droplets in homogeneous isotropic turbulence. *Phys. Fluids* **21**: 125108, DOI: 10.1063/1.3276906.

Osiptsov AN. 2000. Lagrangian modelling of dust admixture in gas flows. *Astrophys. Space Sci.* **274**: 377–386.

Paluch IR. 1979. The entrainment mechanism in Colorado cumuli. *J. Atmos. Sci.* **36**: 2467–2478.

Paluch IR, Knight CA. 1984. Mixing and the evolution of cloud droplet size spectra in a vigorous continental cumulus. *J. Atmos. Sci.* **41**: 1801–1815.

Pawlowska H, Brenguier J-L. 2003. An observational study of drizzle formation in stratocumulus clouds for general circulation model (GCM) parameterizations. *J. Geophys. Res.* **108**: 8630, DOI: 10.1029/2002JD002679.

Pawlowska H, Brenguier J-L, Burnet F. 2000. Microphysical properties of stratocumulus clouds. *Atmos. Res.* **55**: 15–33.

Peters N. 2000. *Turbulent Combustion*. Cambridge University Press: Cambridge, UK.

Pinsky M, Khain AP. 2001. Fine structure of cloud droplet concentration as seen from the Fast-FSSP measurements. Part I: Method of analysis and preliminary results. *J. Appl. Met.* **40**: 1515–1537.

Pinsky MB, Khain AP. 2002. Effects of in-cloud nucleation and turbulence on droplet spectrum formation in cumulus clouds. *Q. J. R. Meteorol. Soc.* **128**: 501–533.

Pinsky M, Khain AP. 2003. Fine structure of cloud droplet concentration as seen from the Fast-FSSP measurements. Part II: Results of in situ observations. *J. Appl. Met.* **42**: 65–73.

Pinsky MB, Khain AP. 2004. Collisions of small drops in a turbulent flow. Part II: Effects of flow accelerations. *J. Atmos. Sci.* **61**: 1926–1939.

Pinsky MB, Khain AP, Levin Z. 1999a. The role of the inertia of cloud drops in the evolution of the spectra during drop growth by diffusion. *Q. J. R. Meteorol. Soc.* **125**: 553–581.

Pinsky M, Khain AP, Shapiro M. 1999b. Collisions of small drops in a turbulent flow. Part 1: Collision efficiency. Problem formulation and preliminary results. *J. Atmos. Sci.* **56**: 2585–2600.

Pinsky M, Khain AP, Shapiro M. 2001. Collision efficiency of drops in a wide range of Reynolds numbers: effects of pressure on spectrum evolution. *J. Atmos. Sci.* **58**: 742–764.

Pinsky MB, Khain AP, Grits B, Shapiro M. 2006. Collisions of cloud droplets in a turbulent flow. Part III: Relative droplet fluxes and swept volumes. *J. Atmos. Sci.* **63**: 2123–2139.

Pinsky MB, Khain AP, Shapiro M. 2007. Collisions of cloud droplets in a turbulent flow. Part IV: Droplet hydrodynamic interaction. *J. Atmos. Sci.* **64**: 2462–2482.

Pinsky M, Khain A, Krugliak H. 2008a. Collisions of cloud droplets in a turbulent flow. Part V: Application of detailed tables of turbulent collision rate enhancement to simulation of droplet spectra evolution. *J. Atmos. Sci.* **65**: 357–374.

Pinsky M, Magaritz L, Khain A, Krasnov O, Sterkin A. 2008b. Investigation of droplet size distributions and drizzle formation using a new trajectory ensemble model. Part I: Model description and first results in a nonmixing limit. *J. Atmos. Sci.* **65**: 2064–2086.

Politovich MK, Cooper WA. 1988. Variability of the supersaturation in cumulus clouds. *J. Atmos. Sci.* **45**: 1651–1664.

Prabha TV, Khain A, Maheshkumar RS, Pandithurai G, Kulkarni JR, Konwar M, Goswami BN. 2011. Microphysics of pre-monsoon and monsoon clouds as seen from in situ measurements during the Cloud Aerosol Interaction and Precipitation Enhancement Experiment (CAIPEEX). *J. Atmos. Sci.* **68**: 1882–1901.

Pruppacher HR, Klett JD. 1997. *Microphysics of Clouds and Precipitation*. Kluwer: Dordrecht.

Randall DA. 1980. Conditional instability of the first kind upside-down. *J. Atmos. Sci.* **37**: 125–130.

Reade WC, Collins LR. 2000. Effect of preferential concentration on turbulent collision rates. *Phys. Fluids* **12**: 2530–2540.

Rodts SMA, Duynkerke PG, Jonker HJJ. 2003. Size distributions and dynamical properties of shallow cumulus clouds from aircraft observations and satellite data. *J. Atmos. Sci.* **60**: 1895–1912.

Rogers RR, Yau MK. 1989. *A Short Course in Cloud Physics*. Butterworth-Heinemann: Woburn, MA.

Saffman PG, Turner JS. 1956. On the collision of drops in turbulent clouds. *J. Fluid Mech.* **1**: 16–30.

Salazar JPLC, de Jong J, Cao L, Woodward SH, Meng H, Collins LR. 2008. Experimental and numerical investigation of inertial particle clustering in isotropic turbulence. *J. Fluid Mech.* **600**: 245–256.

Saw EW, Shaw RA, Ayyalasomayajula S, Chuang PY, Gylfason A. 2008. Inertial clustering of particles in high-Reynolds-number turbulence. *Phys. Rev. Lett.* **100**: 214501, DOI: 10.1103/PhysRevLett.100.214501.

Sedunov YS. 1974. *Physics of Drop Formation in the Atmosphere*. Wiley: New York.

Seifert A, Nuijens L, Stevens B. 2010. Turbulence effects on warm-rain autoconversion in precipitating shallow convection. *Q. J. R. Meteorol. Soc.* **136**: 1753–1762.

Shaw RA. 2000. Supersaturation intermittency in turbulent clouds. *J. Atmos. Sci.* **57**: 3452–3456.

Shaw RA. 2003. Particle–turbulence interactions in atmospheric clouds. *Annu. Rev. Fluid Mech.* **35**: 183–227.

Shaw RA, Oncley SP. 2001. Acceleration intermittency and enhanced collision kernels in turbulent clouds. *Atmos. Res.* **59–60**: 77–87.

Shaw RA, Reade WC, Collins LR, Verlinde J. 1998. Preferential concentration of cloud droplets by turbulence: effects on the early evolution of cumulus cloud droplet spectra. *J. Atmos. Sci.* **55**: 1965–1976.

Shaw RA, Reade WC, Collins LR, Verlinde J. 1999. Reply to comments on 'Preferential concentration of cloud droplets by turbulence: effects on the early evolution of cumulus cloud droplet spectra'. *J. Atmos. Sci.* **56**: 1437–1441.

Shaw RA, Kostinski AB, Larsen ML. 2002. Towards quantifying droplet clustering in clouds. *Q. J. R. Meteorol. Soc.* **128**: 1043–1057.

Shima S, Kusano K, Kawano A, Sugiyama T, Kawahara S. 2009. The super-droplet method for the numerical simulation of clouds and precipitation: a particle-based and probabilistic microphysics model coupled with a non-hydrostatic model. *Q. J. R. Meteorol. Soc.* **135**: 1307–1320.

Shy SS, Breidenthal RE. 1990. Laboratory experiments on the cloud-top entrainment instability. *J. Fluid Mech.* **214**: 1–15.

Sidin RSR, IJzermans RHA, Reeks MW. 2009. A Lagrangian approach to droplet condensation in atmospheric clouds. *Phys. Fluids* **21**: 106603, DOI: 10.1063/1.3244646.

Siebert H, Lehmann K, Wendisch M. 2006a. Observations of small-scale turbulence and energy dissipation rates in the cloudy boundary layer. *J. Atmos. Sci.* **63**: 1451–1466.

Siebert H, Franke H, Lehmann K, Maser R, Saw EW, Schell D, Shaw RA, Wendisch M. 2006b. Probing finescale dynamics and microphysics of clouds with helicopter-borne measurements. *Bull. Am. Meteorol. Soc.* **87**: 1727–1738.

Siebert H, Shaw RA, Warhaft Z. 2010a. Statistics of small-scale velocity fluctuations and internal intermittency in marine stratocumulus clouds. *J. Atmos. Sci.* **67**: 262–273.

Siebert H, Gerashchenko S, Gylfason A, Lehmann K, Collins LR, Shaw RA, Warhaft Z. 2010b. Towards understanding the role of turbulence on droplets in clouds: in situ and laboratory measurements. *Atmos. Res.* **97**: 426–437.

Siems ST, Bretherson CS, Baker MB, Shy S, Breidenthal RE. 1990. Buoyancy reversal and cloud-top entrainment instability. *Q. J. R. Meteorol. Soc.* **116**: 705–739.

Slawinska J, Grabowski WW, Pawlowska H, Morrison H. 2011. Droplet activation and mixing in large-eddy simulation of a shallow cumulus field. *J. Atmos. Sci.* DOI: 10.1175/JAS-D-11-054.1.

Smoluchowski M. 1916. Drei Vortraege ueber Diffusion, Brownsche Bewegung und Koagulation von Kolloidteilchen. *Phys. Z.* **17**: 557–585.

Snider JR, Guibert S, Brenguier J-L, Putaud J-P. 2003. Aerosol activation in marine stratocumulus clouds: 2. Köhler and parcel theory closure studies. *J. Geophys. Res.* **108**: 8629, DOI: 10.1029/2002JD002692.

Squires KD, Eaton JK. 1990. Particle response and turbulence modification in isotropic turbulence. *Phys. Fluids A* **2**: 1191–1203.

Squires P. 1952. The growth of cloud drops by condensation. *Aust. J. Sci. Res.* **5**: 59–86.

Squires P. 1958. Penetrative downdraughts in cumuli. *Tellus* **10**: 381–389.

Squires P, Turner JS. 1962. An entraining jet model for cumulo-nimbus updraughts. *Tellus* **14**: 422–434.

Srivastava RC. 1989. Growth of cloud drops by condensation: a criticism of currently accepted theory and a new approach. *J. Atmos. Sci.* **46**: 869–887.

Stevens B. 2002. Entrainment in stratocumulus-topper mixed layers. *Q. J. R. Meteorol. Soc.* **128**: 2663–2690.

Stevens B. 2006. Bulk boundary-layer concepts for simplified models of tropical dynamics. *Theor. Comput. Fluid Dyn.* **20**: 279–304.

Stevens B, Feingold G, Cotton WR, Walko RL. 1996. Elements of the microphysical structure of numerically simulated nonprecipitating stratocumulus. *J. Atmos. Sci.* **53**: 980–1006.

Stevens B, Moeng C-H, Ackerman AS, Bretherson CS, Chlond A, de Roode S, Edwards J, Golaz J-C, Jiang H, Khairoutdinov M, Kirkpatrick MP, Lewellen DC, Lock A, Müller F, Stevens DE, Whelan E, Zhu P. 2005. Evaluation of large-eddy simulations via observations of nocturnal marine stratocumulus. *Mon. Weather Rev.* **133**: 1443–1462.

Su C-W, Krueger SK, McMurtry PA, Austin PH. 1998. Linear eddy modeling of droplet spectral evolution during entrainment and mixing in cumulus clouds. *Atmos. Res.* **47–48**: 41–58.

Sundaram S, Collins LR. 1997. Collision statistics in an isotropic particle-laden turbulent suspension. Part 1: Direct numerical simulations. *J. Fluid Mech.* **335**: 75–109.

Tennekes H. 1968. Simple model for the small-scale structure of turbulence. *Phys. Fluids* **11**: 669–671.

Turner JS. 1966. Jets and plumes with negative and reversing buoyancy. *J. Fluid Mech.* **26**: 779–792.

Turner JS. 1973. *Buoyancy Effects in Fluids*. Cambridge University Press: Cambridge, UK.

Twomey S. 1959. The nuclei of natural cloud formation. Part II: The supersaturation in natural clouds and the variation of cloud droplet concentration. *Geofis. Pura Appl.* **43**: 243–249.

Vaillancourt PA, Yau MK. 2000. Review of particle-turbulence interactions and consequences for cloud physics. *Bull. Am. Meteorol. Soc.* **81**: 285–298.

Vaillancourt PA, Yau MK, Grabowski WW. 2001. Microscopic approach to cloud droplet growth by condensation. Part I: Model description and results without turbulence. *J. Atmos. Sci.* **58**: 1945–1964.

Vaillancourt PA, Yau MK, Bartello P, Grabowski WW. 2002. Microscopic approach to cloud droplet growth by condensation. Part II: Turbulence, clustering and condensational growth. *J. Atmos. Sci.* **59**: 3421–3435.

van Zanten MC, Stevens , Nuijens L, Siebesma AP, Ackerman AS, Burnet F, Cheng A, Couvreux F, Jiang H, Khairoutdinov M, Kogan Y, Lewellen DC, Mechem D, Nakamura K, Noda A, Shipway BJ, Slawinska J, Wang S, Wyszogrodzki A. 2011. Controls on precipitation and cloudiness in simulations of trade-wind cumulus as observed during RICO. *J. Adv. Model. Earth Syst.* **3**: M06001, DOI: 10.1029/2011MS000056.

Vohl O, Mitra SK, Wurzler SC, Pruppacher HR. 1999. A wind tunnel study of the effects of turbulence on the growth of cloud drops by collision and coalescence. *J. Atmos. Sci.* **56**: 4088–4099.

Wang L-P, Grabowski WW. 2009. The role of air turbulence in warm rain initiation. *Atmos. Sci. Lett.* **10**: 1–8.

Wang L-P, Maxey MR. 1993. Settling velocity and concentration distribution of heavy particles in homogeneous isotropic turbulence. *J. Fluid Mech.* **256**: 27–68.

Wang L-P, Wexler AS, Zhou Y. 1998a. Statistical mechanical descriptions of turbulent coagulation. *Phys. Fluids* **10**: 2647–2651.

Wang L-P, Wexler AS, Zhou Y. 1998b. On the collision rate of small particles in isotropic turbulence. I. Zero-inertia case. *Phys. Fluids* **10**: 266–276.

Wang L-P, Wexler AS, and Zhou Y. 2000. Statistical mechanical descriptions of turbulent coagulation of inertial particles. *J. Fluid Mech.* **415**: 117–153.

Wang L-P, Ayala O, Grabowski WW. 2005a. Improved formulations of the superposition method. *J. Atmos. Sci.* **62**: 1255–1266.

Wang L-P, Ayala O, Karsprzak SE, Grabowski WW. 2005b. Theoretical formulation of collision rate and collision efficiency of hydrodynamically interacting cloud droplets in turbulent atmosphere. *J. Atmos. Sci.* **62**: 2433–2450.

Wang L-P, Ayala O, Xue Y. 2005c. Reconciling the cylindrical formulation with the spherical formulation in the kinematic descriptions of collision kernel. *Phys. Fluids* **17**: 067103.

Wang L-P, Ayala O, Xue Y, Grabowski WW. 2006a. Comments on 'Droplets to drops by turbulent coagulation'. *J. Atmos. Sci.* **63**: 2397–2401.

Wang L-P, Xue Y, Ayala O, Grabowski WW. 2006b. Effects of stochastic coalescence and air turbulence on the size distribution of cloud droplets. *Atmos. Res.* **82**: 416–432.

Wang L-P, Franklin CN, Ayala O, Grabowski WW. 2006c. Probability distributions of angle of approach and relative velocity for colliding droplets in a turbulent flow. *J. Atmos. Sci.* **63**: 881–900.

Wang L-P, Ayala O, Rosa B, Grabowski WW. 2008. Turbulent collision efficiency of heavy particles relevant to cloud droplets. *New J. Phys.* **10**: 075013, DOI: 10.1088/1367-2630/10/7/075013.

Wang Y, Geerts B, French J. 2009. Dynamics of the cumulus cloud margin: an observational study. *J. Atmos. Sci.* **66**: 3660–3677.

Warhaft Z. 2009. Laboratory studies of droplets in turbulence: towards understanding the formation of clouds. *Fluid Dyn. Res.* **41**: 011201, DOI: 10.1088/0169-5983/41/1/011201.

Warner J. 1955. The water content of cumuliform cloud. *Tellus* **7**: 449–457.

Warner J. 1969a. The microstructure of cumulus clouds. Part I: General features of the droplet spectrum. *J. Atmos. Sci.* **26**: 1049–1059.

Warner J. 1969b. The microstructure of cumulus clouds. Part II: The effect on droplet size distribution of the cloud nucleus spectrum and updraft velocity. *J. Atmos. Sci.* **26**: 1272–1282.

Warner J. 1970. On steady-state one-dimensional models of cumulus convections. *J. Atmos. Sci.* **27**: 1035–1040.

Westerweel J, Fukushima C, Pedersen JM, Hunt JCR. 2009. Momentum and scalar transport at the turbulent/non-turbulent interface of a jet. *J. Fluid Mech.* **631**: 199–230.

Wilkinson M, Mehlig B. 2005. Caustics in turbulent aerosols. *Europhys. Lett.* **71**: 186–192.

Wilkinson M, Mehlig B, Bezuglyy V. 2006. Caustic activation of rain showers. *Phys. Rev. Lett.* **97**: 048501, DOI: 10.1103/PhysRevLett. 97.048501.

Woittiez EJP, Jonker HJJ, Portela LM. 2009. On the combined effects of turbulence and gravity on droplet collisions in clouds: a numerical study. *J. Atmos. Sci.* **66**: 1926–1943.

Wood AM, Hwang W, Eaton JK. 2005. Preferential concentration of particles in homogeneous and isotropic turbulence. *Int. J. Multiphase Flow* **31**: 1220–1230.

Wyszogrodzki AA, Grabowski WW, Wang L-P. 2011. Activation of cloud droplets in bin-microphysics simulation of shallow convection. *Acta Geophys.* **59**: 1168–1183.

Xue Y, Wang L-P, Grabowski WW. 2008. Growth of cloud droplets by turbulent collision–coalescence. *J. Atmos. Sci.* **65**: 331–356.

Yamaguchi T, Randall DA. 2008. Large-eddy simulation of evaporatively driven entrainment in cloud-topped mixed layers. *J. Atmos. Sci.* **65**: 1481–1504.

Yang TS, Shy SS. 2005. Two-way interaction between solid particles and homogeneous air turbulence: particle settling rate and turbulence modification measurements. *J. Fluid Mech.* **526**: 171–216.

Zaichik LI, Alipchenkov VM. 2003. Pair dispersion and preferential concentration of particles in isotropic turbulence. *Phys. Fluids* **15**: 1776–1787.

Zhou Y, Wexler AS, Wang L-P. 2001. Modelling turbulent collision of bidisperse inertial particles. *J. Fluid Mech.* **433**: 77–104.